Journal of Space Operations & Communicator (ISSN 2410-0005)
Vol. 18, No. 3, Year 2022

Hybrid-Equivalences while Coupling Anomalistic with Draconitic Satellite Motions

Ernst Friedrich Maria Jochim[1]

German Aerospace Centre, Oberpfaffenhofen, Germany

Abstract: The orbital motions of the celestial bodies, to which also the Earth satellites are to be counted, can be considered under different orbital reference frames. One particular aspect is considered in the present paper. Two different motions are each coupled together by causing the differences between the orbital periods in question to vanish. The orbit obtained, which unifies the special properties of the two types of motion, is called an equivalence orbit. Numerically, within the framework of a trajectory selection, it is checked whether the difference between the two orbital periods falls below a certain predefined accuracy barrier. If the bound is smaller than about 10**-9 sec, the obtained orbit shall be called an exact equivalence orbit. However, there are also orbits which combine the properties of the two motions with a good approximation, although the difference between their period times does not fall below the accuracy limit of about 0.01sec. Such orbits shall be called near-parallel equivalence orbits. The present paper deals with the equivalence between anomalistic and draconitic motions. As in many cases of equivalence orbits, also in the case of equivalence between anomalistic and draconitic motions there is a characteristic inclination, in the vicinity of which equivalence orbits can occur exclusively. In this case the characteristic inclination is equal to the critical inclination. Now, in the case of equivalence between anomalistic and draconitic motions, it surprisingly turns out that the inclinations of all exact equivalence orbits are below the characteristic inclination, while close near-parallel equivalence orbits with accuracy limits below 0.01sec usually have inclinations above the critical inclination. We will refer to this case of equivalence orbits as hybrid-equivalence orbits. As in any case of equivalence orbits, if five orbit parameters are preselected, the sixth parameter can be calculated with the equivalence condition. In the case of exact equivalence orbits, the sixth parameter can be calculated with extremely high accuracy. In the present case, this is possible for inclinations below the characteristic inclination. Otherwise, the accuracy of the calculated parameter is lower. Typical for hybrid-equivalence orbits is the smooth transition from exact to near-parallel equivalence orbits. An interesting property of equivalence orbits, which are formed by the coupling of anomalistic with draconitic motion, is their long-term stability over the Earth's surface: the perigee of the orbit moves over long times (years in terms of magnitude) stably over one and the same parallel of latitude (analogous for the apogee). This stability is maintained particularly long on exact equivalence orbits, not so long only approximately on near-parallel equivalence orbits, which must be stabilized then occasionally with orbit corrections.

[1] Dr. Ing., Dipl. Math., retired scientific coworker, Tel: (+49)-8153-28-2738, Fax: (+49)-8153-28-1452, e-mail: Fritz.Jochim@dlr.de, German Aerospace Center (DLR), Microwave and Radar Institute, Oberpfaffenhofen Muenchner Str. 20, D-82234 Weßling, Germany, ORCID: 0000-0002-9861-7062

Keywords: Equivalence orbits; Coupling of satellite motions; Anomalistic motion; Draconitic motion; Exact equivalence orbits; Near-parallel equivalence orbits; Hybrid-equivalence orbits; Special influence of J_4

Table of Symbols:

a	semimajor axis [km]
$\bar{a}$	mean semimajor axis [km]
$\bar{a}_0$	mean epoch semimajor axis [km]
$\overline{a_{QAD}}$	mean semimajor axis of a $\left(\overline{P_A} \triangleq \overline{P_D}\right)$ – resp. $\left(P_A \triangleq P_D\right)$ – equivalence orbit as computed with equivalence condition
e	eccentricity
e_B	boundary eccentricity for demarcating an area of possible equivalence orbits
$\bar{e}_0$	mean epoch eccentricity
$\overline{e_{QAD}}$	eccentricity of a $\left(\overline{P_A} \triangleq \overline{P_D}\right)$ – resp. $\left(P_A \triangleq P_D\right)$ – equivalence orbit as computed with equivalence condition
G	equal area parameter [km^2/s] (in case of conic section orbits: $G = \sqrt{\mu p}$)
H_P	perigee height [km]
i	inclination [deg]
$\bar{i}_0$	mean epoch inclination [deg]
$\overline{i_{QAD}}$	inclination [deg] of a $\left(\overline{P_A} \triangleq \overline{P_D}\right)$ – resp. $\left(P_A \triangleq P_D\right)$ – equivalence orbit as computed with equivalence condition
$\left(i\right)^{\bullet}_s$	secular variation of inclination [rad/sec]
J_2, J_3, J_4, J_5	zonal harmonic potential coefficients $\left(J_2 = 1.082625379977 \times 10^{-3}\right)$ $\left(J_3 = -2.5320063539269 \times 10^{-6}\right)$ $\left(J_4 = -1.61969083203 \times 10^{-6}\right)$ (see, e.g., Urban and Seidelmann, 2013).
$M_0, \overline{M_{00}}$	mean anomaly at epoch [deg], mean mean anomaly at epoch [deg]
$\left(M_0\right)^{\bullet}_s$	secular variation of mean epoch anomaly [rad/sec]
$\left(M_0\right)^{\bullet}_{Gs}$	secular variation of mean epoch anomaly [rad/sec] in Earth's gravitational field including effects due to J_2, J_4 of *Brouwer*s orbital model
$\overline{n_A}, n_A$	mean, true anomalistic satellite mean motion [rad/sec]
$\overline{n_D}, n_D$	mean, true draconitic satellite mean motion [rad/sec]
$\overline{n_K}$	*Kepler*ian mean motion [rad/sec], $\overline{n_K} = \sqrt{\mu / \bar{a}^3}$
$\overline{n_{K0}}$	*Kepler*ian mean motion [rad/sec] related to epoch, $\overline{n_{K0}} = \sqrt{\mu / \bar{a}_0^3}$
$\overline{n_R}, n_R$	mean, true meridional satellite mean motion [rad/sec]
p	semilatus rectum [km]
$\overline{P_A}, P_A$	mean, true anomalistic period [sec]
$\overline{P_D}, P_D$	mean, true draconitic period [sec]

$\overline{P_K}, P_K$	mean, true *Kepler*ian period [sec], $\overline{P_K} = \sqrt{\mu / \overline{a}^3}$, $P_K = \sqrt{\mu / a^3}$
$\overline{P_R}, P_R$	mean, true meridional period [sec], $\overline{P_R} = 2\pi / \overline{n_R}$
$\overline{P_S}, P_S$	mean, true Sun synodic period [sec]
$\left(\overline{P_A} \triangleq \overline{P_d}\right) -$	equivalence orbit for coupling between mean anomalistic and mean draconitic satellite motion
$\left(P_A \triangleq P_d\right) -$	equivalence orbit for coupling between true anomalistic and true draconitic satellite motion
R_E	mean equatorial radius of Earth (R_E =6378.1366 km)
r	radius [km]
t	time [sec] (in universal time UT1)
t_0	epoch time
u	argument of latitude [rad]
V	velocity [km/s]
α	right ascension of satellite [deg or rad]
δ	declination of satellite [deg or rad]
δ_p	periodic part of any parameter, e.g. $\alpha = \overline{\alpha} + \delta_p \alpha$
λ	geographic longitude [rad]
λ_P	geographic longitude of orbital perigee [rad]
$\dot{\lambda}_{Ps}$	secular drift of geographic longitude of orbital perigee [rad/sec]
Δa	Step size for semimajor axis [km]
$\Delta(a)$	Accuracy for semimajor axis [km]
Δe	Step size for eccentricity
$\Delta(e)$	Accuracy for eccentricity
Δi	Step size for inclination [deg]
$\Delta(i)$	Accuracy for inclination [deg]
$\overline{\Delta\lambda_P}$	shift [rad] of geographic longitude of orbital perigee per mean anomalistic period
$\overline{\Delta\lambda_\Omega}$	shift [rad] of geographic longitude of ascending node per mean draconitic period
λ	(eastern) geographic longitude [deg]
λ_P	geographic longitude of perigee [deg or rad]
λ_Ω	geographic longitude of ascending node [deg or rad]
$\dot{\lambda}_{\Omega s}$	secular drift of geographic longitude of ascending node [rad/sec]
μ, $\mu_{\oplus}$	gravitational constant of the central body [km^3/sec^2], of the Earth ($\mu_{\oplus}$=398600.4418000 km^3 / sec^2)
φ	geodetic latitude [deg]
σ_i	retrograde factor: $\sigma_i = \mathrm{sgn}\left(\cos i\right)$
Θ_G	sidereal time at Greenwich meridian [deg]
Θ_{G0}	sidereal time at midnight Greenwich meridian [deg]

$\dot{\Theta}$	tropical rotational rate of Earth [rad/sec]: $\dot{\Theta}$ [WGS84] $= 0.7291158573340 \times 10^{-4}$ / s (J2000.0)
υ	true anomaly [deg]
υ_p	periodic part in development of true anomaly
ω	argument of perigee [deg]
$\bar{\omega}_0$	mean epoch argument of perigee [deg]
$\dot{\omega}_s$	secular variation of argument of perigee [rad/sec]
$\dot{\omega}_{Gs}$	secular variation of argument of perigee [rad/sec] in Earth's gravitational field including effects due to J_2, J_4 of *Brouwer*s orbital model
$\dot{\omega}_{Gs/1}$	part of the J_2-component of $\dot{\omega}_{Gs}$
$\dot{\omega}_{Gs/2}$	part of the J_2^2-component of $\dot{\omega}_{Gs}$
$\dot{\omega}_{Gs/4}$	part of the J_4 – component of $\dot{\omega}_{Gs}$
Ω	right ascension of ascending node [deg]
$\bar{\Omega}_0$	mean epoch right ascension of ascending node [deg]
$\dot{\Omega}_s$	secular variation of right ascension of ascending node [rad/sec]
$\dot{\Omega}_{Gs}$	secular variation of right ascension of ascending node [rad/sec] in Earth's gravitational field including effects due to J_2, J_4 of *Brouwer*s orbital model

- In the tables of orbital parameters, red numbers mark exact equivalences, green numbers mark near-parallel equivalences.

1 Introduction: equivalence orbits

The orbital motion of a satellite can be considered from different points of view. Each of these types of motion is characterized by a reference point. Such a reference point can be the perigee of the orbit, the ascending node, the vernal equinox, the Sun, the Moon, a special arbitrarily chosen and then fixed point on the satellite orbit in the context of a *Hansen* motion (Jochim, 2012). Each of such motion is described by an orbit angle aligned to the reference point as the starting point of its count.

If two such types of motion are coupled, special satellite orbits are obtained. We call these orbits “equivalence orbits”. These orbits are characterized by a more or less large orbital stability over long periods of time. To study them, the trajectory of the orbital period in question is considered versus the semimajor axis. There are cases where the curves of the orbital periods have a precise irreversibly unique intersection point which can be determined with great accuracy. The difference between the two orbital periods at this point can be determined numerically to an accuracy of 10^{-9} seconds or better. These types of equivalence orbits are characterized as "exact equivalence orbits." There are also cases where the curves of the orbital periods do not intersect, but are nearly parallel. They can approximate each other with some accuracy, say on the order of 10^{-2} seconds. These orbits can also have the properties of equivalence orbits, albeit with less accuracy and not over as long a time period as the exact equivalence orbits. These orbits are referred to as "near-parallel equivalence orbits."

The investigations are carried out in the present work with the analytical orbital model of *D. Brouwer* (Brouwer 1959). In this model the *Kepler* elements are decomposed into a secular and periodic part with respect to the zonal harmonics J_2, J_3, J_4, J_5 of the Earth's gravity field. In the applications of satellite orbital mechanics, the part with J_5 is usually not considered.

Two complementary methods of calculating equivalence orbits are considered. If only the secular parts are considered in the representations of the *Kepler* elements, a mean motion is obtained. They result in a "mean equivalence orbit", which already shows the essential properties of an equivalence orbit. If the whole orbit model with all periodic parts is included in the investigation, a "true equivalence orbit" is obtained. The calculation is much more complex by calculating the respective orbit angles. Usually, it can only be carried out iteratively with numerical methods. Mostly, it deepens the results of the mean equivalence orbit only minimally.

There are now equivalence orbits which, depending on the choice of an orbital parameter, such as inclination, can be both exact and close parallel equivalence orbits. The present study is devoted to such a case. We will refer to these types of equivalence orbits as "hybrid-equivalence orbits".

Results in satellite orbit mechanics are usually improved when higher perturbations are taken into account. In the present context, however, in the given orbital mechanics environment, a different result can be obtained in principle when higher perturbations are taken into account. This phenomenon is investigated in detail in this study.

2 Characteristics of anomalistic to draconitic equivalence orbits

2.1 Computation of anomalistic and draconitic periods

The motion on satellite orbits characterized on the perigee as reference point is called anomalistic orbit motion. The associated orbit angle is the true anomaly υ. It can be decomposed into a mean component $\overline{n_A} = \overline{n_K} + \left(M_0\right)^{\bullet}_s$ and a periodic component υ_p. In *Brouwer*'s theory mean *Kepler*ian elements at an epoch t_0 are input parameters for the secular as well as the periodic evolutions. The mean *Kepler*ian motion at an epoch t_0 is given applying the mean epoch semimajor axis $\overline{a}_0$ by $\overline{n_{K\,0}} := \sqrt{\mu / \overline{a}_0^3}$. The secular variation $\left(M_0\right)^{\bullet}_s$ of the mean epoch mean anomaly is given in *Brouwer* (1959). The mean anomalistic orbital period is

$$\overline{P_A} = 2\pi / \overline{n_A} \ . \tag{1}$$

The true anomalistic period P_A can be calculated (usually iteratively) with the superimposed function

$$fct\left(P_A\right) \equiv \sin\left[\upsilon\left(t_0 + P_A\right) - \upsilon\left(t_0\right)\right] = 0 \ . \tag{2}$$

As initial value $P_A^{(0)} := \overline{P_A}$ can be used from formula (1) or e.g. *Kepler*'s orbital period $\overline{P_K} = 2\pi / \overline{n_K}$.

The draconitic satellite motion is characterized by the reference to the ascending node Ω of the orbit. It uses the argument of the latitude $u = \upsilon + \omega$ as orbital angle. ω is the argument of the perigee with the secular variation $\dot{\omega}_s$. The mean draconitic motion and the mean draconitic orbital period are

$$\overline{n_D} = \overline{n_K} + \left(M_0\right)_s^{\cdot} + \dot{\omega}_s \quad , \quad \overline{P_D} = 2\pi / \overline{n_D} \quad . \tag{3}$$

The true draconitic period P_D can be calculated (again, usually iteratively) with the superimposed function

$$fct\left(P_D\right) \equiv \sin\left[u\left(t_0 + P_A\right) - u\left(t_0\right)\right] = 0 \ . \tag{4}$$

Notes: 1. For the calculation of the zero, e.g. $\upsilon\left(t_0 + P_A\right) = \upsilon\left(t_0\right)$, the sine function is used here as a "superimposed" function. It has the same zero as the original function, but can be calculated more unambiguously and numerically more stable and has a very large convergence interval (approximately in the range (-85°, +85°)).

2. The here used formulas of orbital mechanics can be found in every textbook of orbital mechanics. They are derived and examined in detail with the designations used here for example in (Jochim 2018).

2.2 Selection of equivalence orbits

Equivalence orbits coupling anomalistic and draconitic motions are denoted by the symbol $\left(\overline{P_A} \triangleq \overline{P_D}\right)$ – equivalence orbits for coupling mean anomalistic orbital periods $\overline{P_A}$ with mean draconitic orbital periods $\overline{P_D}$. Correspondingly are $\left(P_A \triangleq P_D\right)$ – equivalence orbits for coupling true (i.e., including all relevant periodic perturbation equations of the orbital model used) anomalistic orbital periods P_A with true draconitic orbital periods P_D .

Two of the mean basic *Kepler*ian orbit parameters $\left(\overline{a}_0, \overline{e}_0, \overline{i}_0\right)$ must be fixed, the third can be calculated considering the $\left(\overline{P_A} \triangleq \overline{P_D}\right)$ – equivalence condition

$$\overline{P_A} - \overline{P_D} = \frac{2\pi}{\overline{\overline{n_A}}} - \frac{2\pi}{\overline{\overline{n_D}}} = 0 \quad . \tag{5}$$

By specifying the eccentricity $\overline{e}_0$ and inclination $\overline{i}_0$, for example, the corresponding semimajor axis $\overline{a_{QAD}}$ can be computed by applying the mean orbital periods P_A, P_D from (1) and (3) with the condition function

$$fct\left(\overline{a}_0^{(\nu)}\right) \equiv \overline{P_A}\left(\overline{a}_0^{(\nu)}\right) - \overline{P_D}\left(\overline{a}_0^{(\nu)}\right) = \frac{2\pi}{\overline{n_A}\left(\overline{a}_0^{(\nu)}\right)} - \frac{2\pi}{\overline{n_D}\left(\overline{a}_0^{(\nu)}\right)} = 0 \quad \left\langle \nu = 1, 2, 3, \cdots \right. . \tag{6}$$

If no first approximation is available, a search process must be started. First, the first approximation can be used with respect to a minimum perigee height, e.g. $H_P := 200\,\text{km}$,

$$\bar{a}_0^{(0)} := \frac{R_E + 200}{1 - \bar{e}_0} \quad . \tag{7}$$

This value is then increased step by step with a preset step size Δa [km].

$$\bar{a}_0^{(\nu+1)} = \bar{a}_0^{(\nu)} + \Delta a \ , \quad \nu = 0,1,2,3,\cdots \quad . \tag{8}$$

According to Figure 1 and Figure 2, the difference $\left|\overline{P_A} - \overline{P_D}\right|$ between the mean anomalistic $\overline{P_A}$ and the mean draconitic orbital period $\overline{P_D}$ decreases with increasing semimajor axis $\bar{a}$ at fixed eccentricity $\bar{e}_0$ and inclination $\bar{i}_0$. If this difference falls below a required accuracy $\Delta\bar{P}$ [sec]

$$\left|\overline{P_A} - \overline{P_D}\right| \le \Delta\bar{P} \quad , \tag{9}$$

the last step value of the semimajor axis after ν steps of iteration can be taken as the final result $\overline{a_{QAD}} := \bar{a}_0^{(\nu)}$. If the equivalence condition (9) cannot be achieved with the selected step size Δa, a refinement with the semimajor axis accuracy Δ(a) can lead to success. As a consequence, it can be seen that the result $\overline{a_{QAD}}$ depends not only on the equivalence condition (9), but also on the step size Δa, the accuracy limit Δ(a) of the semimajor axis, and the limit accuracy $\Delta\bar{P}$ (for example, see after formula (15)).

In an analogous way the semimajor axis of a **true** $\left(P_A \triangleq P_D\right)$ – **equivalence orbit** can be calculated for given *Kepler*ian elements $\left(\bar{e}_0, \bar{i}_0, \bar{\Omega}_0, \bar{\omega}_0, \overline{M}_{00}\right)$. To do this, an initial approximation $\bar{a}_0^{(0)}$ (such as from formula (7)) is used to calculate the true orbital periods P_A, P_D with the conditional equations (2) and (4):

$$fct\left(P_A\right) \equiv \sin\left[\upsilon\left(t_0 + P_A\right) - \upsilon\left(t_0\right)\right] = 0 \ , \ fct\left(P_D\right) \equiv \sin\left[u\left(t_0 + P_A\right) - u\left(t_0\right)\right] = 0 \quad . \tag{10}$$

With the computed true orbital periods, an improved semimajor axis can be obtained with a selected step size Δa, the semimajor axis accuracy Δ(a) and using the equivalence condition equation

$$fct\left(\bar{a}_0^{(\nu)}\right) \equiv P_D\left(\bar{a}_0^{(\nu)}\right) - P_A\left(\bar{a}_0^{(\nu)}\right) = 0 \qquad \langle \nu = 1,2,3,\cdots . \tag{11}$$

The whole process (10) - (11) must be iterated several times until for a required function accuracy ΔP [sec], inclusive a step size Δa and the accuracy limit Δ(a) of the semimajor axis, the condition

$$\left|P_A - P_D\right| \le \Delta P \tag{12}$$

is fulfilled. The final result yields $\overline{a_{QAD}} := \overline{a}_0^{(\nu)}$. Similar to the case of mean $\left(\overline{P_A} \triangleq \overline{P_D}\right)-$equivalence orbits, this result depends on the step size Δa, the accuracy limit Δ(a) of the semimajor axis and the limit accuracy ΔP on the equivalence condition (12).

Remarks:

1. In analogous way, also the orbital elements eccentricity or inclination can be computed with the corresponding equivalence conditions.
2. In the algorithm presented here only mean orbit elements are used for both mean and true equivalence orbits. The reason is the *Brouwer* orbit model used, which applies only mean orbit elements as parameters to calculate the perturbed orbit data. If another orbit model or a numerical orbit propagator is used, the corresponding orbit parameters must be adjusted. There should be no fundamental change in the process presented for calculating an equivalence orbit.
3. The orbit parameters used here are uniquely assigned to each other in a reversible way within the framework of an equivalence problem. In principle, this assignment can be read off from the overview representation of exact $\left(\overline{P_A} \triangleq \overline{P_D}\right)-$equivalence orbits in Figure 10 (see in section 3.3).

2.3 General characteristics of anomalistic with draconitic equivalence orbits

In this section, we summarize the particular characteristics of an equivalence orbit resulting from the coupling of anomalistic and draconitic satellite orbital motions.

To construct an $\left(\overline{P_A} \triangleq \overline{P_D}\right)-$equivalence orbit, the mean anomalistic motion must be coupled with the mean draconitic motion. Therefore, the necessary and sufficient condition is

- *the **first property** of* $\left(\overline{P_A} \triangleq \overline{P_D}\right)-$*equivalence orbits*

$$\overline{n_D} = \overline{n_A} + \dot{\omega}_s \to \overline{n_A} \quad \Leftrightarrow \dot{\omega}_s = 0 \quad \Leftrightarrow \quad \overline{P_D} = \frac{2\pi}{\overline{n_D}} = \frac{2\pi}{\overline{n_A}} = \overline{P_A} \quad . \tag{13}$$

The secular drift of the argument of the perigee due to the gravitational field (G) of the Earth is given in *Brouwer*'s theory (Brouwer 1959) by the expression

$$\begin{aligned}\dot{\omega}_{Gs} \quad = \quad & -\frac{3}{4}\,\overline{n_{K\,0}}\,J_2\,\frac{R_E^2}{\overline{p}_0^2}\left(1-5\cos^2\overline{i}_0\right)+\\ & +\frac{3}{2^7}\,\overline{n_{K\,0}}\,\frac{R_E^4}{\overline{p}_0^4}\left\{J_2^2\left[-35+24\sqrt{1-\overline{e}_0^2}+25\left(1-\overline{e}_0^2\right)+\right.\right.\\ & \qquad +\left(90-192\sqrt{1-\overline{e}_0^2}-126\left(1-\overline{e}_0^2\right)\right)\cos^2\overline{i}_0+\\ & \qquad \left.+\left(385+360\sqrt{1-\overline{e}_0^2}+45\left(1-\overline{e}_0^2\right)\right)\cos^4\overline{i}_0\right]-\\ & \qquad -5\,J_4\left[21-9\left(1-\overline{e}_0^2\right)+\left(-270+126\left(1-\overline{e}_0^2\right)\right)\cos^2\overline{i}_0+\right.\\ & \qquad \left.\left.+\left(385-189\left(1-\overline{e}_0^2\right)\right)\cos^4\overline{i}_0\right]\right\}+\dots\ .\end{aligned} \tag{14}$$

Based on condition (13), it shows that for Earth satellite orbits in first order accuracy $\left[O\left(J_2\right)\right]$ the inclination is close to the *characteristic inclinations*

$$1-5\cos^2 i_{char}=0 \;\;\Rightarrow\;\; i_{char1}=63^\circ.434949,\; i_{char2}=116^\circ.565051 \;\; . \tag{15}$$

EXAMPLE: The semimajor axis of a $\left(\overline{P_a}\triangleq\overline{P_d}\right)-$equivalence orbit with minimum perigee height $H_P=200$ km and the given eccentricity $\overline{e}_0$=0.35 is to be determined. According to expression (15), the given inclination must be close to the characteristic inclination $i_{char\,1}$. Let it be chosen $\overline{i}_0$= 63°.428.

The functional equation (6) is processed with the step size Δa = 1 km, the functional accuracy $\Delta\overline{P}$ = 10^{-8} sec and the accuracy Δ(*a*) = 10^{-7} km of the semimajor axis. The computation is done with the whole *Brouwer*'s orbit model. The solution is:

$$\overline{a_{QAD\,0}} = 15996.326155 \text{ km}$$

with the orbital periods and the achieved accuracy

$\overline{P_A}$ = 20135.7874417 sec, $\overline{P_D}$ = 20135.7874417 sec, $\overline{P_a}-\overline{P_d}=0.9829818736762\times10^{-8}$ sec.

Notes:

1. In the analytical orbit theory of *D. Brouwer* (Brouwer, D. 1959), these values of inclination are usually called "critical inclinations" $i_{crit}=i_{char}$ (see, e.g., (Breakwell 1959)). They appear with the expression $\left(1-5\cos^2 i\right)$ as vanishing denominators in the case $i=i_{crit}$ in the long-period perturbation equations of the *Kepler*ian elements. However, in the context of the present theory of $\left(\overline{P_A}\triangleq\overline{P_D}\right)-$ and $\left(P_A\triangleq P_D\right)-$ equivalence orbits, orbits near the "critical" inclinations are not critical.
2. The critical inclinations are independent of any other orbital parameter. However, considering the whole expression (14), in the context of the theory of $\left(\overline{P_A}\triangleq\overline{P_D}\right)-$equivalence orbits, the characteristic inclinations $i_{char\,1}, i_{char\,2}$ necessarily depend also on the semimajor axis $\overline{a}_0$ and the eccentricity $\overline{e}_0$ (see e.g. Figure 10).

3. Also, in the case of other equivalence orbits, which can be formed by coupling of two different satellite motions, which are neither anomalistic nor draconitic, characteristic inclinations occur. These have completely different values than the critical inclination.
4. To avoid confusion and uncertainty, the term "critical inclination" is generally avoided in this paper in the context of anomalistic with draconitic $\left(\overline{P_A} \triangleq \overline{P_D}\right)-$equivalence orbits.

From expression (14) it is clear that orbits with inclinations close to the characteristic inclination are essentially influenced by second-order formula components in J_2^2 and J_4 of magnitude 10^{-6}. Therefore, in all investigations of $\left(\overline{P_A} \triangleq \overline{P_D}\right)-$equivalence orbits, the full mathematical expression available must be considered.

The secular drift $\dot{\lambda}_{\Omega s} = \dot{\Omega}_s - \dot{\Theta}$ of the geographic nodal longitude can be compared with the secular drift of the geographic longitude of the perigee

$$\dot{\lambda}_{Ps} = \dot{\Omega}_s + \frac{\cos \overline{i}_0}{1-\sin^2 \overline{i}_0 \cos^2 \overline{\omega}_0}\,\dot{\omega}_s - \frac{\sin \overline{i}_0 \sin \overline{\omega}_0 \cos \overline{\omega}_0}{1-\sin^2 \overline{i}_0 \cos^2 \overline{\omega}_0}\,(i)^{\bullet}_{\ s} - \dot{\Theta} \quad . \tag{16}$$

(see, e.g., in (Jochim, 2018, chap. 22.9.2)).

The orbits in the neighborhood of the characteristic inclinations $i_{char\,1}, i_{char\,2}$ are of the order of $\left|\dot{\omega}_s\right| \ll 1.0$. For near-Earth satellite orbits, the secular drift of the inclination is $\left|(i)^{\bullet}_s\right| \ll 1.0$ (Klinkrad, 1985). Due to the equivalence condition (5), the mean shift in nodal longitude per mean draconitic orbital period and the mean shift in perigee longitude per mean anomalistic period can be approximately equalized. With $\dot{\omega}_s \approx 0.0$ and $(i)^{\bullet}_{\ s} \approx 0.0$ formula (16) results directly

- *the **second property** of $\left(\overline{P_A} \triangleq \overline{P_D}\right)-$equivalence orbits*

$$\overline{\Delta\lambda_{\Omega}} = \dot{\lambda}_{\Omega s}\,\overline{P_d} \approx \dot{\lambda}_{Ps}\,\overline{P_a} = \overline{\Delta\lambda_P} \qquad \langle \overline{i}_0 \approx i_{char\,1/2} \quad . \tag{17}$$

Because of $\left|\dot{\omega}_s\right| \ll 1.0$, there are for the secular development of the argument of the perigee

$$\overline{\omega} = \overline{\omega}_0 + \dot{\omega}_s \left(t - t_0\right) \tag{18}$$

no significant changes over long periods of time (for practical applications, this time frame is on the order of years). It can thus be assumed $\overline{\omega} \approx \overline{\omega}_0$. The apsides and thus the whole subsatellite orbit of a satellite are displaced parallel to the Earth's surface for a long time. As a consequence

- *the **third property** of $\left(\overline{P_A} \triangleq \overline{P_D}\right)-$equivalence orbits: In the case of equivalence between anomalistic and draconitic motion, the perigee (just as the apogee) of the orbit moves along a fixed parallel of latitude of the Earth's body.*

A quantitative example is presented in section 3.2. See e.g. Figure 9.

2.4 Special characteristics of anomalistic to draconitic equivalence orbits

To get an overview of the possible $\left(\overline{P_A} \triangleq \overline{P_D}\right)$ – equivalence orbits, the difference $\overline{P_A} - \overline{P_D}$ versus the semimajor axis for selected orbit inclinations is shown in Figure 1. For first investigations, only circular orbits are considered.

The result is astonishing: For orbits with inclinations larger than the characteristic inclination $i_{char\,1}$, the difference $\overline{P_A} - \overline{P_D}$ decreases with increasing semimajor axis. The difference never disappears. Orbits with inclinations greater than the characteristic inclination $i_{char\,1}$ are therefore always near-parallel $\left(\overline{P_A} \triangleq \overline{P_D}\right)$ – equivalence orbits.

However, orbits with inclinations smaller than the characteristic inclination $i_{char\,1}$ can show exactly $\overline{P_A} = \overline{P_D}$. These orbits are exact $\left(\overline{P_A} \triangleq \overline{P_D}\right)$ – equivalence orbits. A detailed overview of possible exact equivalence orbits is calculated in Figure 10. All these calculations are performed with the complete *Brouwer* orbit model (Brouwer 1959).

Another interesting fact is shown in Figure 2. The calculations for this figure were performed analogously to the calculations for Figure 1, with the exception that only the influence of J_2 und J_2^2 was taken into account. The influences of J_4 are thus truncated. No zero points can be observed, not even for orbits with inclinations smaller than the characteristic inclination $i_{char\,1}$. In this case only near-parallel equivalence orbits are possible.

If in the expression (14) the influences of J_4 are truncated, the influences of J_2^2 are still included in the calculations. One has to keep in mind that J_2^2 is of the order 10^{-6}, thus of the same order as that of J_4. In the above calculations, however, one gets the impression that the influences of J_2^2 have no effect, while those of J_4 do. This strange behavior will be examined in more detail in the next section.

Notes:

1. The investigations carried out here are related only to the characteristic inclination $i_{char\,1}$. However, they can also be directed to the characteristic inclination $i_{char\,2}$ in a mirrored way.
2. In analytical investigations of satellite orbital motions, the consideration of higher orbital models can not only inevitably lead to an improved numerical statement, but also to a fundamentally new statement. So far, no other equivalence orbit with a similar behavior has been found as in the present case of $\left(\overline{P_A} \triangleq \overline{P_D}\right)$ – equivalence orbits.

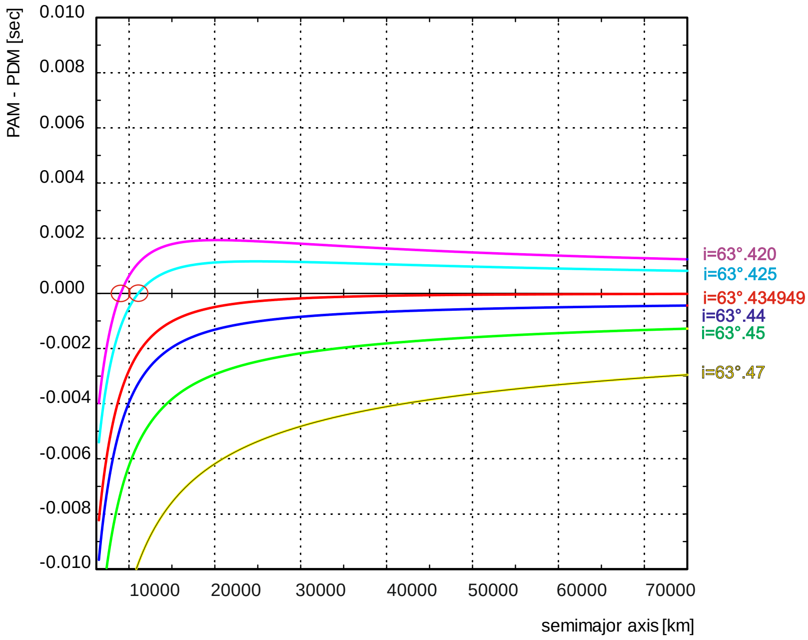

Figure 1: Curves of the difference $\left(\overline{P_A} - \overline{P_D}\right)$ in mean orbital periods $\overline{P_A}, \overline{P_D}$ of circular orbits versus the semimajor axis for various inclinations in the vicinity of the characteristic inclination $i_{char\,1}$. The J_2, J_3, J_4 perturbations of the orbital motion are included in the calculations. The zero points $\left(\overline{P_A} = \overline{P_D}\right)$ are marked. Exact $\left(\overline{P_A} \triangleq \overline{P_D}\right)$ – equivalence orbits occur only at these points.

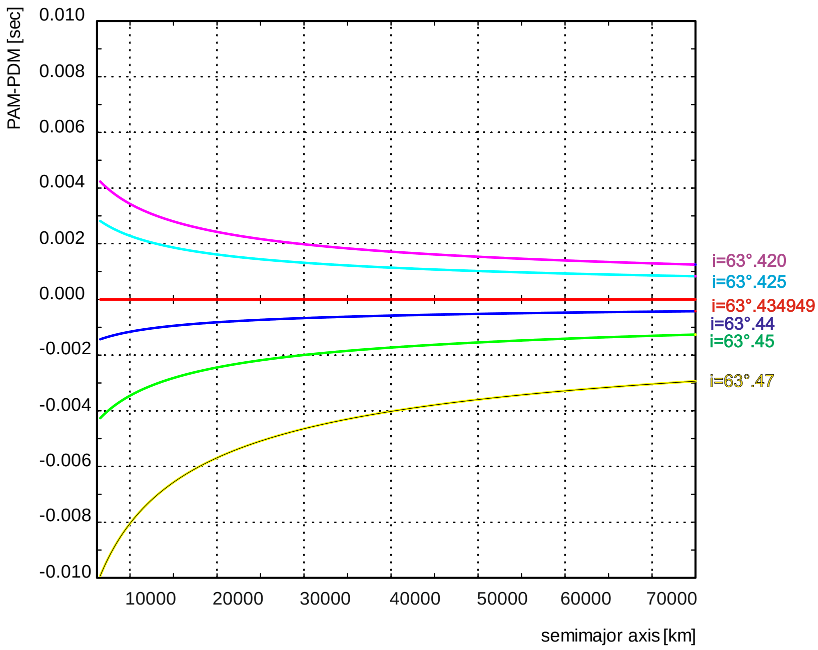

Figure 2: Curves of the difference $\left(\overline{P_A} - \overline{P_D}\right)$ of the mean orbital periods $\overline{P_A}, \overline{P_D}$ of circular orbits versus the semimajor axis for different inclinations in the vicinity of the characteristic inclination $i_{char\,1}$. Only the J_2 und J_2^2 perturbations of the orbital motion are included in the calculation. There are no zero points $\left(\overline{P_A} = \overline{P_D}\right)$. Thus, only near-parallel $\left(\overline{P_A} \triangleq \overline{P_D}\right)$ – equivalence orbits occur.

3 Exact anomalistic with draconitic equivalence orbits

3.1 The influence of the fourth zonal harmonic

In order to study the individual influences of J_2, J_2^2 and J_4 on the behavior of orbits in the vicinity of the characteristic inclinations, the expression (14) is decomposed into three distinct parts:

$$\dot{\omega}_{Gs/1} \;:=\; -\frac{3}{4}\,\overline{n_{K\,0}}\,J_2\,\frac{R_E^2}{\overline{p}_0^2}\left(1-5\cos^2\overline{i}_0\right) \tag{19}$$

$$\begin{aligned}\dot{\omega}_{Gs/2} \;:=\; +\frac{3}{2^7}\,\overline{n_{K\,0}}\,\frac{R_E^4}{\overline{p}_0^4}\,J_2^2\Big\{&-35+24\sqrt{1-\overline{e}_0^2}+25\left(1-\overline{e}_0^2\right)+\\ &+\left(90-192\sqrt{1-\overline{e}_0^2}-126\left(1-\overline{e}_0^2\right)\right)\cos^2\overline{i}_0+\\ &+\left(385+360\sqrt{1-\overline{e}_0^2}+45\left(1-\overline{e}_0^2\right)\right)\cos^4\overline{i}_0\Big\}\end{aligned} \tag{20}$$

$$\begin{aligned}\dot{\omega}_{Gs/4} \;:=\; -\frac{15}{2^7}\,\overline{n_{K\,0}}\,\frac{R_E^4}{\overline{p}_0^4}\,J_4\Big\{&\,21-9\left(1-\overline{e}_0^2\right)+\left(-270+126\left(1-\overline{e}_0^2\right)\right)\cos^2\overline{i}_0+\\ &+\left(385-189\left(1-\overline{e}_0^2\right)\right)\cos^4\overline{i}_0\Big\}\end{aligned} \tag{21}$$

Figure 3 illustrates these three components above the inclination in the vicinity of the characteristic inclination for a circular orbit with a minimum altitude of 200 km. Obviously, the influence of the considered component $\dot{\omega}_{Gs/2}$ with J_2^2 compared to the part $\dot{\omega}_{Gs/4}$, which contains J_4, can be neglected. The difference between these two parts decreases with increasing eccentricity, but will never disappear. This can be concluded from Figure 4 and Figure 5.

In all three figures, the curve of the fraction $\dot{\omega}_{Gs/1}$ with J_2 alone is shown in blue color. The curve of the proportion $\dot{\omega}_{Gs/1}+\dot{\omega}_{Gs/2}$ with $J_2+J_2^2$ has the color cyan. This cyan curve overlaps more or less completely with the blue J_2-curve. Consequently, in the framework investigated in this study, the contribution of the J_2^2-component can be neglected. Due to the dominance of the J_2-component, the influence of the $\dot{\omega}_{Gs/1}+\dot{\omega}_{Gs/2}$-part of $J_2+J_2^2$ disappears almost exactly at the characteristic inclination $i_{char\,1}$.

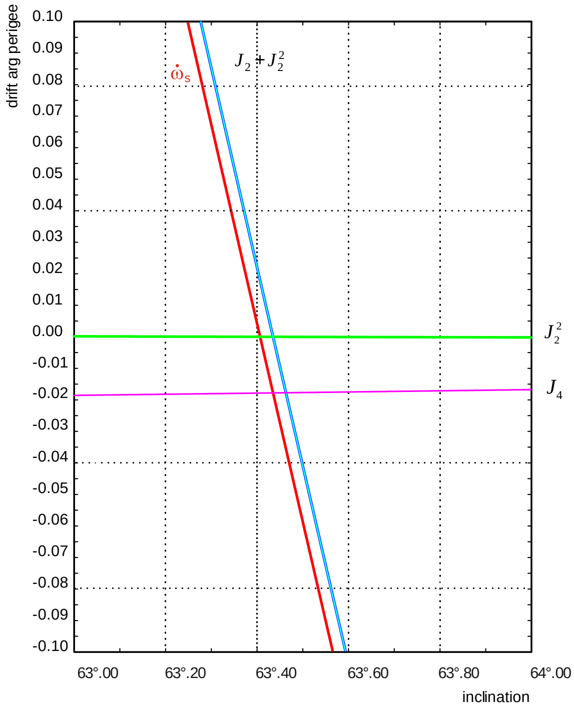

Figure 3: The secular drift of the argument of perigee $\left(\dot{\omega}_{Gs} \times 10^7 \text{ rad/sec}\right)$ and its individual components due to J_2, J_2^2, J_4 depending on the inclination near the characteristic inclination, circular orbit with the semimajor axis 6367.140 km Red curve: $\dot{\omega}_{Gs}$ blue: part with J_2 and $J_2 + J_2^2$, green: part with J_2^2 exact at the zero line, magenta: part with J_4 alone below the zero line

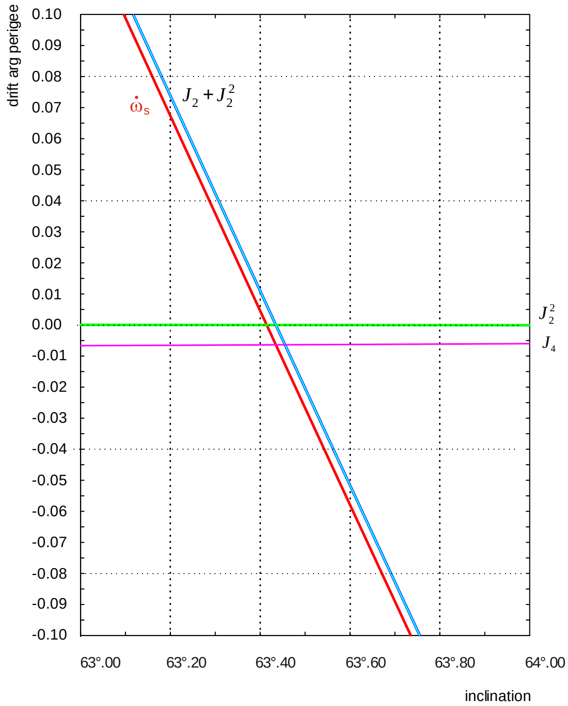

Figure 4: The secular drift of the argument of perigee $\left(\dot{\omega}_{Gs} \times 10^7 \text{ rad/sec}\right)$ and its individual components due to J_2, J_2^2, J_4 depending on the inclination near the characteristic inclination, eccentric orbit e=0.2 , with the semimajor axis 8222.67125 km. Red curve: $\dot{\omega}_{Gs}$ blue: part with J_2 and $J_2 + J_2^2$, green: part with J_2^2 alone exact at the zero line, magenta: part with J_4 alone below the zero line

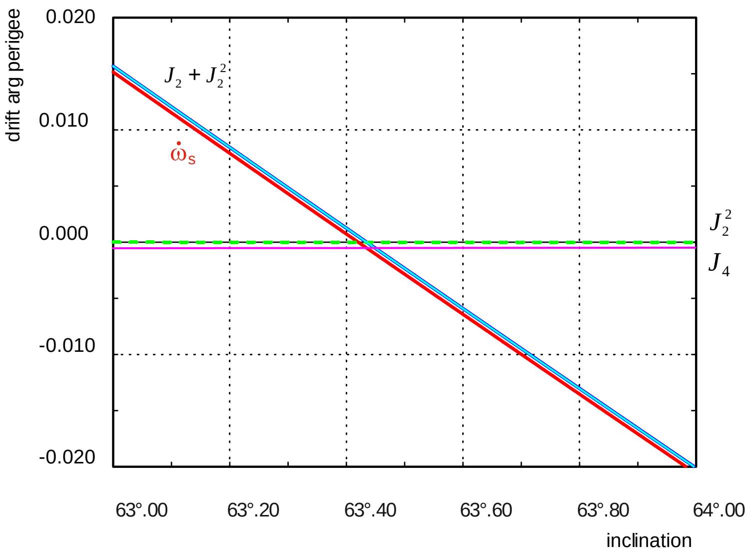

Figure 5: The secular drift of the argument of perigee $\left(\dot{\omega}_{Gs} \times 10^7 \text{ rad/sec}\right)$ and its individual components due to J_2, J_2^2, J_4 depending on the inclination near the characteristic inclination, eccentric orbit e=0.7, with the semimajor axis 21927.123333 km. Red curve: $\dot{\omega}_{Gs}$, blue: part with J_2 and $J_2 + J_2^2$, green: part with J_2^2 alone exact at the zero line, magenta: part with J_4 alone slightly below the zero line.

eccentricity	$\overline{a_{Qad}}$ [km]	J_2^2-part	J_4-part	$\bar{i}_0\left[J_2+J_2^2\right]$	$\bar{i}_0\left[\dot{\omega}_{Gs}\right]$
0.0	6578.140	-2.0×10^{-4}	-2.0×10^{-2}	63°.435	63°.407
0.1	7309.041	-1.0×10^{-4}	-1.0×10^{-2}	63°.435	63°.411
0.2	8222.671	-8.0×10^{-5}	-6.0×10^{-3}	63°.435	63°.415
0.3	9397.339	-5.0×10^{-5}	-4.0×10^{-3}	63°.435	63°.417
0.4	10963.562	-4.0×10^{-5}	-3.0×10^{-3}	63°.435	63°.418
0.5	13156.274	-3.0×10^{-6}	-1.0×10^{-3}	63°.435	63°.419
0.6	16445.343	-3.0×10^{-6}	-1.0×10^{-4}	63°.435	63°.420
0.7	21927.123	-1.0×10^{-6}	-5.0×10^{-4}	63°.435	63°.421
0.8	32890.685	-2.0×10^{-7}	-3.0×10^{-4}	63°.435	63°.421
0.9	65781.370	-3.0×10^{-8}	-8.0×10^{-5}	63°.435	63°.421
0.0	21927.123	-2.0×10^{-7}	-2.0×10^{-5}	63°.435	63°.411

Table 3-1: The influence of J_4 on the inclination of a $\left(\overline{P_A}\triangleq\overline{P_D}\right)$ – equivalence orbit in the context of the characteristic inclination, for orbits with different eccentricities. The semimajor of the orbit is chosen with respect to the perigee height of 200 km. In addition, the J_4-influence on a circular high-altitude orbit is shown in the last line. The inclination is chosen with the step size $\Delta i=\left(10^{-4}\right)$ degrees.

To obtain the total secular variation $\dot{\omega}_{Gs}$ of the argument of the perigee, the $\dot{\omega}_{Gs/4}$-part of the J_4-component is added to the $\dot{\omega}_{Gs/1}+\dot{\omega}_{Gs/2}$-part of $J_2+J_2^2$. The total $\dot{\omega}_{Gs}=\dot{\omega}_{Gs/1}+\dot{\omega}_{Gs/2}+\dot{\omega}_{Gs/4}$-curve runs below the $\dot{\omega}_{Gs/1}+\dot{\omega}_{Gs/2}$-curve with the $J_2+J_2^2$-component because of the negative sign of the $\dot{\omega}_{Gs/4}$-part with J_4. For this reason, in this case the zero point of the $\dot{\omega}_{Gs}$-curve can only be determined for inclinations smaller than the characteristic inclination $i_{char\,1}$. According to condition (13) $\dot{\omega}_s\triangleq\dot{\omega}_{Gs}=0.0$ rad/sec, the condition for an exact $\left(\overline{P_A}\triangleq\overline{P_D}\right)$ – equivalence orbit is fulfilled.

The corresponding values for discrete values of eccentricities $\in\left[0.0,0.9\right)$ are compiled in Table 1. The semimajor axes are chosen to produce orbits with a minimum perigee height of 200 km. The table contains the approximate values for the J_2^2- and the J_4-components, the zero point for the $J_2+J_2^2$-component, i.e. the characteristic inclination $i_{char\,1}$, and the zero point for the entire $\dot{\omega}_{Gs}$-curve. This point corresponds to the inclination of an exact equivalence orbit.

For comparison, the table additionally contains a circular orbit with the semimajor axis $\overline{a_{Q\,0}}$=21927.123 km.

3.2 Properties of exact anomalistic with draconitic equivalence orbits

For a more detailed investigation of the exact $\left(\overline{P_A} \triangleq \overline{P_D}\right)$ – equivalence orbits, the difference $\overline{P_A} - \overline{P_D}$ between the mean anomalistic and the mean draconitic orbital period versus the semimajor axis is investigated. Figure 6 is a section of Figure 1 showing the progression of circular orbits. Correspondingly, Figure 7 shows the course of an eccentric orbit. In both cases, the orbits are shown with different inclinations.

According to the previous considerations, all these orbits must have smaller inclinations than the characteristic inclination $i_{char\,1}$. Exact $\left(\overline{P_A} \triangleq \overline{P_D}\right)$ – equivalence orbits occur in the zero points $\left|\overline{P_A} - \overline{P_D}\right| = 0$. All orbits are performed using the full *Brouwer*'s orbit model. Figure 8 shows, for some given inclinations, all exact $\left(\overline{P_A} \triangleq \overline{P_D}\right)$ – equivalence orbits versus various eccentricities and semimajor axes. An extreme example is the curve with inclination $\overline{i}_0$ = 63°.410. According to Figure 6, circular exact $\left(\overline{P_A} \triangleq \overline{P_D}\right)$ – equivalence orbits are possible for all semimajor axes. However, Figure 7 shows that orbits with eccentricity $\overline{e}_0$ = 0.3 and with inclination $\overline{i}_0$ = 63°.410 can never be exact $\left(\overline{P_A} \triangleq \overline{P_D}\right)$ – equivalence orbits. This is illustrated by Figure 8: the curve of exact $\left(\overline{P_A} \triangleq \overline{P_D}\right)$ – equivalence orbits with inclination $\overline{i}_0$ =63°.410 ends at eccentricity $\overline{e}_0$ = 0.07.

Table 2 contains the orbit parameters for some exact $\left(\overline{P_A} \triangleq \overline{P_D}\right)$ – equivalence orbits for different inclinations and eccentricities. The search process was performed with the step size $\Delta a = 1\,\text{km}$, the accuracy $\Delta(a) \le 10^{-7}\,\text{km}$ of the semimajor axis and the function accuracy $\left|\Delta\overline{P}\right| = \left|\overline{P_A} - \overline{P_D}\right| \le 10^{-8}\,\text{sec}$. The achieved accuracy $\left(\overline{P_a} - \overline{P_d}\right)[\text{sec}]$ and the value of the secular drift of the argument of the perigee are included in the table. If the condition $\overline{P_A} - \overline{P_D} = 0.0$ is fulfilled, the achieved accuracy in each case can be smaller than $10^{-12}\,\text{sec}$.

EXAMPLE: The semimajor axis of an exact $\left(\overline{P_A} \triangleq \overline{P_D}\right)$ – equivalence orbit with inclination $\overline{i}_0$ =63°.418 and eccentricity $\overline{e}_0$ =0.35 is to be constructed.

The search process for calculating the corresponding semimajor axis with the condition function

$$fct\left(\overline{a_{QAD}}\right) \equiv \overline{P_A}\left(\overline{a}\right) - \overline{P_D}\left(\overline{a}\right) = \frac{2\pi}{\overline{n_A}\left(\overline{a}\right)} - \frac{2\pi}{\overline{n_D}\left(\overline{a}\right)} = 0 \tag{22}$$

starts with an orbit with a minimum perigee of 200 km and the corresponding semimajor axis $\overline{a}_0^{(0)}$ =10120.210154 km.

With the step size Δa=1km and the required function accuracy $\left|\Delta\overline{P}\right| \le 1.0\times10^{-9}\,\text{sec}$ and the accuracy limit for the semimajor axis $\Delta(a) \le 1.0\times10^{-9}\,\text{km}$, the semimajor axis $\overline{a_{QAD}}$ =10245.888 km is obtained considering all orbital influences due to J_2, J_2^2 and J_4.

$\bar{i}_0$	$\bar{e}_0$	$\bar{a}_0\,[\mathrm{km}]$	$\left(\overline{P_a} = \overline{P_d}\right)$ [sec]	$\left(\overline{P_a} - \overline{P_d}\right)[\mathrm{sec}]$	$\dot{\omega}_{Gs}\,[\mathrm{rad/sec}]$
63°.410	0.0	7000.278310	5830.431516	$< 10^{-12}$ sec	$0.48153078588856 \times 10^{-19}$
	0.3	---	---	---	---
	0.6	---	---	---	---
63°.417	0.0	8251.209228	7460.561035	$< 10^{-12}$ sec	$-0.4873014046368 \times 10^{-19}$
	0.3	9462.411894	9161.939926	$< 10^{-12}$ sec	$-0.1519391198531 \times 10^{-19}$
	0.6	---	---	---	---
63°.418	0.35	10245.888986	10322.902654	$< 10^{-12}$ sec	$-0.9485176686568 \times 10^{-21}$
63°.420	0.0	9040.389403	8555.822681	$0.18189894 \times 10^{-11}$	$0.14224394268857 \times 10^{-18}$
	0.3	10367.478636	10507.081620	$< 10^{-12}$ sec	$0.52383254392058 \times 10^{-19}$
	0.6	16450.528302	21000.1365182	$< 10^{-12}$ sec	$-0.1227685955514 \times 10^{-19}$
63°.425	0.0	11079.745704	11607.86526	$< 10^{-12}$ sec	$0.26082710773810 \times 10^{-19}$
	0.3	12706.289499	14255.419404	$< 10^{-12}$ sec	$0.46411553206701 \times 10^{-20}$
	0.6	20161.929391	28492.900556	$< 10^{-12}$ sec	$0.11221028126708 \times 10^{-20}$
63°.430	0.0	15706.868140	19591.542156	$< 10^{-12}$ sec	$-0.1360272021714 \times 10^{-19}$
	0.3	18012.811228	24060.441323	$< 10^{-12}$ sec	$-0.1394653654628 \times 10^{-19}$
	0.6	28582.584443	48092.453754	$< 10^{-12}$ sec	$0.46840055382224 \times 10^{-20}$
63°.434	0.0	35865.137000	67596.495709	$0.8119968697 \times 10^{-8}$	$-0.1116862101037 \times 10^{-16}$
	0.3	41131.338571	83018.360482	$0.5529727786 \times 10^{-8}$	$-0.5035155229558 \times 10^{-17}$
	0.6	65268.342500	165946.266859	$0.4627509042 \times 10^{-8}$	$-0.1057591200615 \times 10^{-17}$

Table 3-2: Orbit parameters of some exact $\left(\overline{P_A} \triangleq \overline{P_D}\right)$ – equivalence orbits for different inclinations and eccentricities. For the search for the semimajor axis, a step size of $\Delta a = 1\,\mathrm{km}$, the accuracy $\Delta(a) \le 10^{-7}$ km and the function accuracy $|\Delta\overline{P}| \le 10^{-8}$ sec were chosen. The orbit model contains the whole *Brouwer* orbit model.

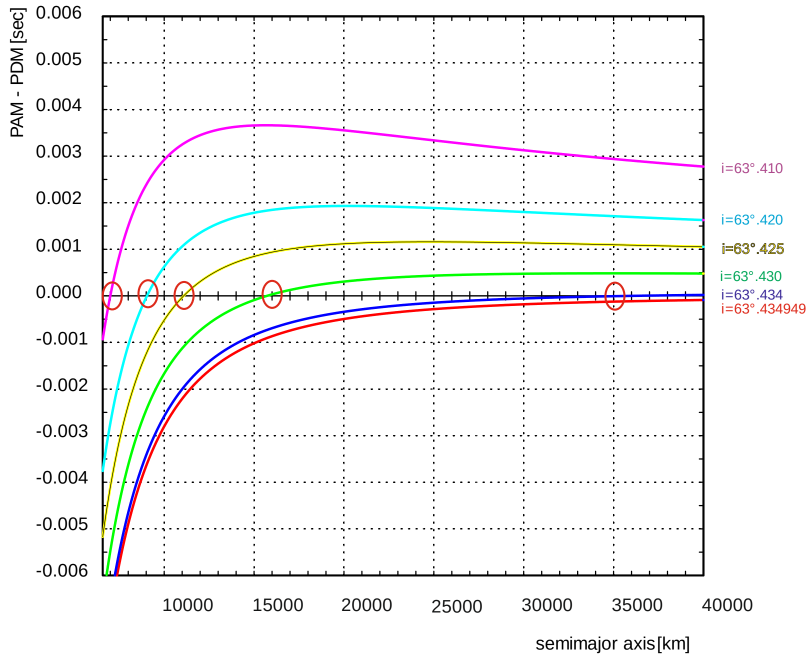

Figure 6 : Curves of the difference $\left(\overline{P_A} - \overline{P_D}\right)$ of the mean orbital periods of circular orbits $\overline{P_A}, \overline{P_D}$ versus the semimajor axis for different inclinations smaller than the characteristic inclination $i_{char\,1}$. The zero points $\left(\overline{P_A} = \overline{P_D}\right)$ are marked. Exact $\left(\overline{P_A} \triangleq \overline{P_D}\right)$ – equivalence orbits occur at these points. Note the red curve for $i_{char1} = 63°.434949$. The calculations are performed using the full *Brouwer*'s orbit model.

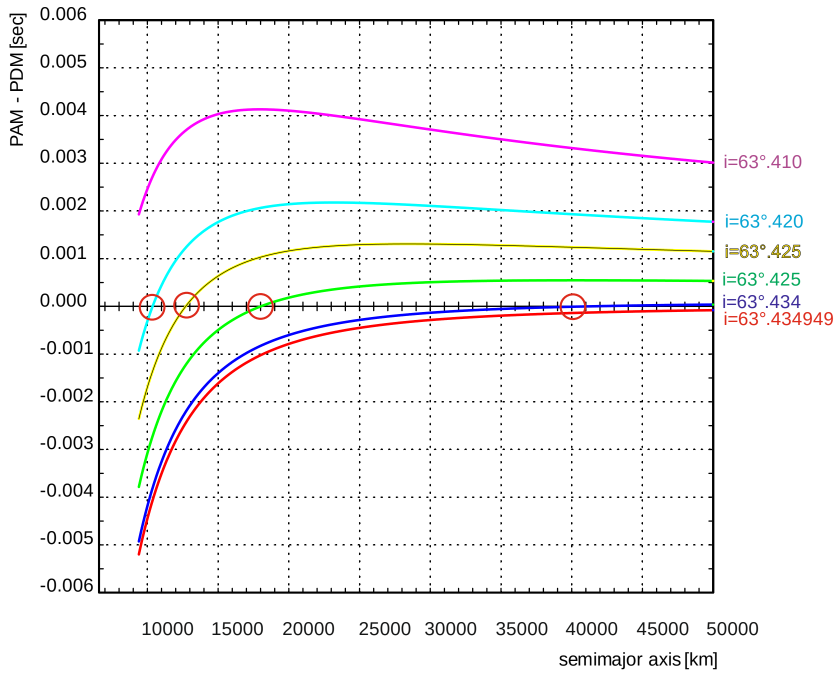

Figure 7 : Curves of the difference $\left(\overline{P_A} - \overline{P_D}\right)$ of the mean orbital periods of eccentric orbits $\overline{P_A}, \overline{P_D}$ with $\left(\overline{e}_0 = 0.3\right)$ versus the semimajor axis for different inclinations smaller than the characteristic inclination $i_{char\,1}$. The zero points $\left(\overline{P_A} = \overline{P_D}\right)$ are marked. Exact $\left(\overline{P_A} \triangleq \overline{P_D}\right)$ – equivalence orbits occur at these points. Note the red curve for $i_{char1} = 63°.434949$. The calculations are performed using the full *Brouwer*'s orbit model.

On the basis of the obtained results, an independent ephemeris calculation gives the mean orbital periods

$$\overline{P_A} = 10322.9016718490075 \text{ sec}, \ \overline{P_D} = 10322.9016718490075 \text{ sec}.$$

The achieved accuracy $\Delta\overline{P} \leq 0.2\times10^{-9}$ sec exceeds the required accuracy. The orbit parameters of this orbit are summarized in Table 3-3. Figure 9 illustrates this orbit and the shift of the perigee (as well as the apogee) along a parallel of latitude.

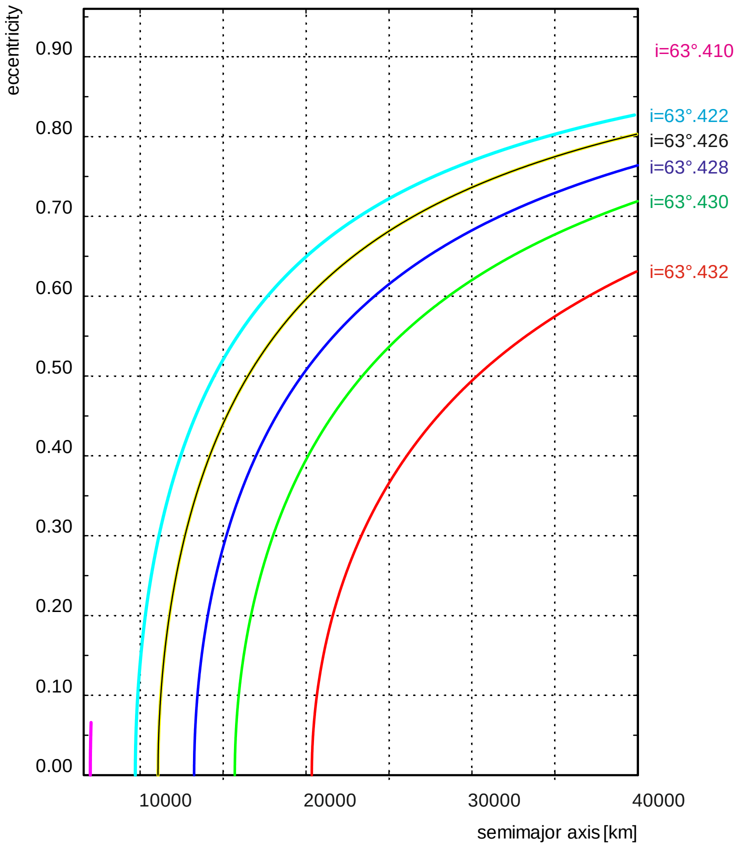

Figure 8: Overview of the eccentricity of the $\left(\overline{P_A} \triangleq \overline{P_D}\right)$ – equivalence orbit families as a function of the semimajor axis for different inclinations smaller than the characteristic inclination $i_{char1} = 63°.434949$. The orbital model contains only the secular perturbations of *Brouwer*'s orbital model.

Note that the condition (17) for the equivalence of the displacement of the mean longitude of the perigee with the displacement of the mean nodal longitude $\overline{\Delta\lambda_P} = \dot{\lambda}_{Ps}\,\overline{P_D} = \overline{\Delta\lambda_\Omega} = \dot{\lambda}_{\Omega s}\,\overline{P_A}$ is also satisfied, as can be read from Table 3-3: the mean argument of the perigee $\bar{\omega}$ according to equation (18) remains quantitatively stable over years. This becomes clear when comparing the secular drift $\dot{\omega}_{Gs}$ of the argument of the perigee in Table 3-3. ◄

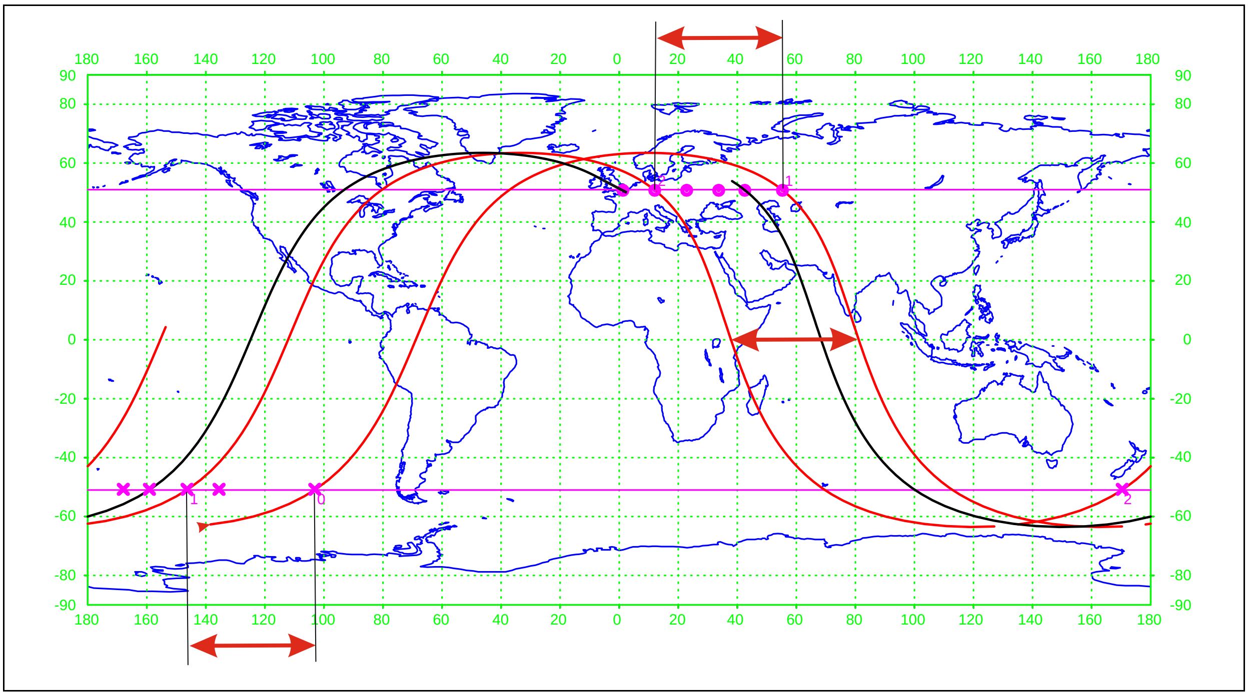

Figure 9: Course of the exact $\left(\overline{P_A} \triangleq \overline{P_D}\right)$ – equivalence orbit with eccentricity $\overline{e}_0$ =0.35, inclination $\overline{i}_0$ =63°.418, right ascension of the ascending node $\overline{\Omega}_0$ =220°, argument of the perigee $\overline{\omega}_0$ =-60°. Shown are the ground tracks of two periods (in red) and one period after one year (in black). The perigees (X) move along the parallel of latitude $\varphi = -51°$, while the apogees (O) move along the parallel of latitude $\varphi = +51°$. The red double arrows mark the shift in the longitude of the ascending node and the shift in the longitude of the perigee per revolution. Both shifts coincide.

$\left(\overline{P_A} \triangleq \overline{P_D}\right)$	
$\overline{a_{QAD}} =$ 10245.888154 km, $\overline{e}_0 = 0.35, \overline{i}_0 = 63°.418, \overline{\Omega}_0 = 0°, \overline{\omega}_0 = 0°, \overline{M}_{00} = 0°$	
$\overline{P_K} = 10321.323649$ sec	t_0 : 2022-01-23/12:00:0.0
$\overline{P_A}$ = 10322.901396 sec	$P_A = 10322.901396$ sec
$\overline{P_D}$ = 10322.901396 sec	$P_D = 10322.901396$ sec
$H_P = 281.690700$ km	$H_A = 7453.812408$ km
$\overline{\Delta\lambda_P} = \dot{\lambda}_P \overline{P_A} = -43°261408$	$\overline{\Delta\lambda_\Omega} = \dot{\lambda}_{\Omega s} \overline{P_D} = -43°262408$
$\Delta\lambda_P = \dot{\lambda}_P P_A = -43°261408$	$\Delta\lambda_\Omega = \dot{\lambda}_{\Omega s} P_D = -43°261408$
$\dot{\omega}_{Gs} = -0.10904499038412693 \times 10^{-16}$ rad/sec	

Table 3-3: Orbit characteristics of an exact $\left(\overline{P_A} \triangleq \overline{P_D}\right)$ – equivalence orbit. Required accuracy $|\Delta\overline{P}| \leq 10^{-7}$ sec, achieved accuracy $\Delta\overline{P} \leq 10^{-13}$ sec. Fundamental parameters used: $R_E = 6378.1366$ km, $\mu_♁ = 398600.4418$ km^3/s^2, $\dot{\Theta}$=0.72921158573340×10^{-4} /s, $J_2 = 0.001082625379977$. The red figures indicate the exact $\left(\overline{P_A} \triangleq \overline{P_D}\right)$ – equivalence. Secular and periodic perturbations are included.

3.3 The domain of exact anomalistic with draconitic equivalence orbits

The representation of the region of possible exact $\left(\overline{P_A} \triangleq \overline{P_D}\right)-$equivalence orbits is computed numerically as follows:

Let the accuracy limit $\Delta\overline{P}$ required for the representation be specified. The inclination $\overline{i}_0$ is considered as an independent parameter. For the search of a $\left(\overline{P_A} \triangleq \overline{P_D}\right)-$equivalence orbit a certain eccentricity $\overline{e}_0$ is chosen in each case. Starting from a minimum semimajor axis $\overline{a}_0^{(0)}$, the mean periods $\overline{P_A}, \overline{P_D}$ are calculated in each step of the inclination $\overline{i}_0$ with the chosen eccentricity $\overline{e}_0$ using the formulas (1) and (3). When the equivalence condition $\left|\overline{P_A} - \overline{P_D}\right| \leq \Delta\overline{P}$ is satisfied, the achieved semimajor axis $\overline{a}_0 =: \overline{a_{QAD}}$ is obtained as the semimajor axis of a $\left(\overline{P_A} \triangleq \overline{P_D}\right)-$equivalence orbit using the condition equation (6). If the equivalence condition is not fulfilled, the fixed values $\left(\overline{e}_0, \overline{i}_0\right)$ are used to increase the semimajor axis by the step size Δa and thus with $\overline{a}_0 \Rightarrow \overline{a}_0 + \Delta a$ calculate new values $\overline{P_A}, \overline{P_D}$. This process is carried out until the equivalence condition is fulfilled with the obtained semimajor axis. Then a new inclination is chosen with the step size $\overline{i}_0 \Rightarrow \overline{i}_0 + \Delta i$ and the whole process is repeated to calculate the appropriate semimajor axis. This process is performed in a given inclination interval.

The computation process for the calculation of the boundary eccentricity e_B also starts with an inclination $\overline{i}_0$ as parameter. However, in this case, starting from the eccentricity $\overline{e}_0^{(0)}$=0.0, the eccentricity is increased with the step size Δe to $\overline{e}_0 \Rightarrow \overline{e}_0 + \Delta e$ until the respectively calculated semimajor axis results in a $\left(\overline{P_A} \triangleq \overline{P_D}\right)-$equivalence orbit which has the specified minimum perigee height H_P. At each step, a refinement can be made using the accuracy limits Δ(a) for the semimajor axis and Δ(e) for the eccentricity, respectively. This process is then repeated for all relevant inclinations.

Figure 10 contains the area of possible exact $\left(\overline{P_A} \triangleq \overline{P_D}\right)-$equivalence orbits with the condition boundary accuracies $\Delta\overline{P} \leq 10^{-11}$ sec, $\Delta(i) \leq 10^{-9}$ deg, $\Delta(a) \leq 10^{-3}$ km, $\Delta(e) \leq 10^{-6}$, the step sizes Δa = 1 km, Δi = 0°.0001, Δe = 0.01 and the minimum perigee height H_P =200 km.

The calculation methods described here can in principle also be performed for true $\left(P_A \triangleq P_D\right)-$equivalence orbits and also with a numerical ephemeris computation.

Note: In Figure 10 the statement is confirmed: exact $\left(\overline{P_A} \triangleq \overline{P_D}\right)-$equivalence orbits are restricted to inclinations smaller than the characteristic inclination $i_{char\,1}$. (Mirrored statement for inclinations larger than the characteristic inclination $i_{char\,2}$).

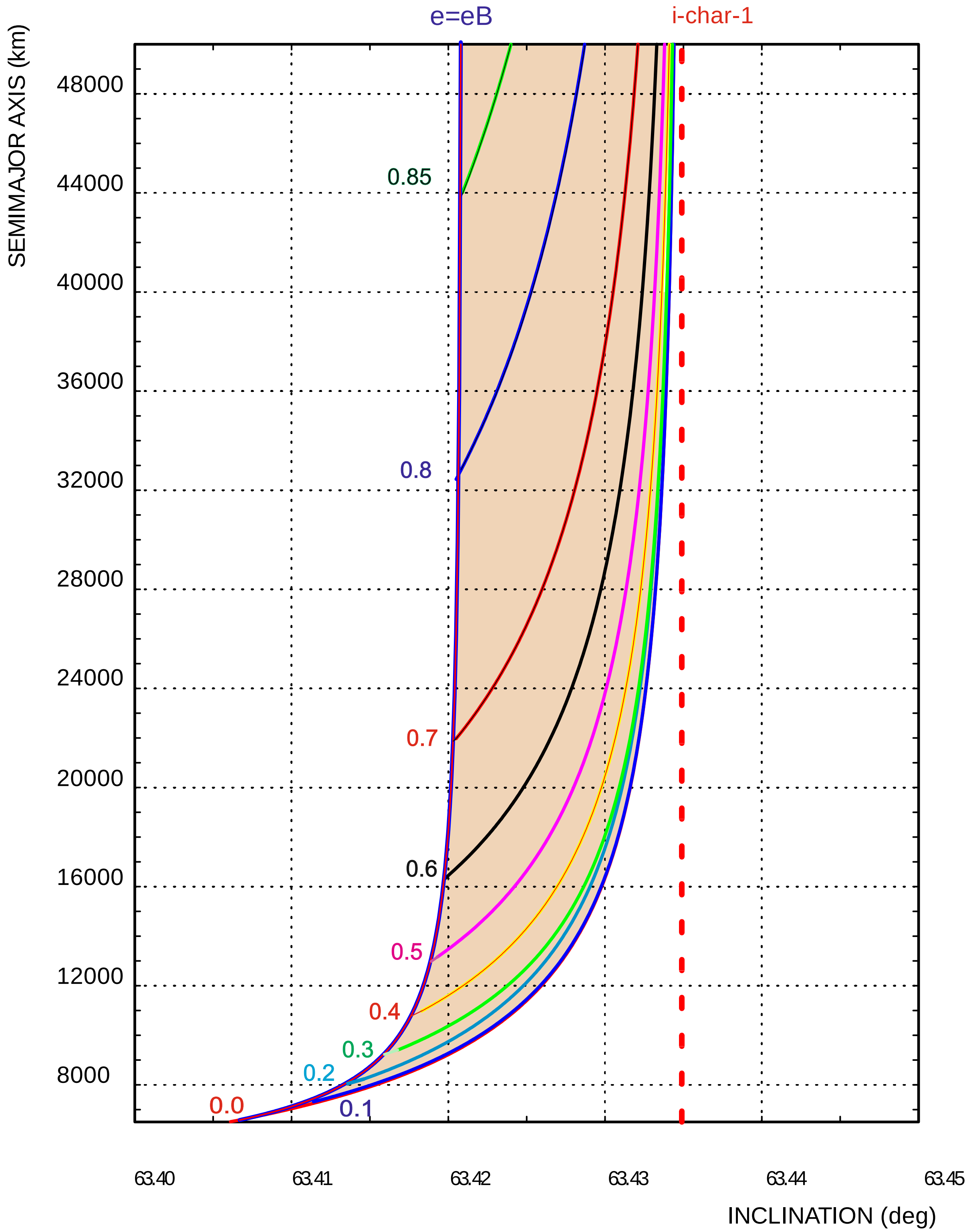

Figure 10: Overview of all exact $\left(\overline{P_A} \triangleq \overline{P_D}\right)$ – equivalence orbits in the semimajor axis range 6578 km < a < 50000 km, with the accuracies $\Delta\overline{P} \leq 10^{-8}$ sec, $\Delta(a) \leq 10^{-3}$ km, $\Delta(e) \leq 10^{-6}$. Step sizes Δa= 1 km, Δ*i* = 0°.0001, Δ*e* = 0.01. Orbit model: *Brouwer* secular orbit model. Fundamental parameters (TCB): $R_E = 6378.1366$ km, $\mu_{♁} = 398600.4356\ \text{km}^3/\text{s}^2$, $\dot{\Theta}[1984] = 0.72921158573340 \times 10^{-4}$ rad/sec, $J_2 = 0.001082625379977$.

3.4 Application for calculating the inclination of an exact anomalistic with draconitic equivalence orbit

The (red) curve for circular exact $\left(\overline{P_A} \triangleq \overline{P_D}\right)-$equivalence orbits in Figure 10 approaches asymptotically to the characteristic inclination $i_{char\,1}$. As the semimajor axis $\overline{a}_0$ grows, the other curves with increasing eccentricity $\overline{e}_0$ tend to approach the characteristic inclination, without reaching it.

If a semimajor axis $\overline{a}_0$ and an eccentricity $\overline{e}_0$<1 are given, the inclination of the corresponding $\left(\overline{P_A} \triangleq \overline{P_D}\right)-$exact equivalence orbits can be calculated using the corresponding equivalence condition. For this purpose, the conditional equations (6) and (11), respectively, are rewritten to the inclination:

$$\begin{aligned} & fct\left(\overline{i}_0^{(\nu)}\right) \equiv \overline{P_A}\left(\overline{i}_0^{(\nu)}\right) - \overline{P_D}\left(\overline{i}_0^{(\nu)}\right) = \frac{2\pi}{\overline{n_A}\left(\overline{i}_0^{(\nu)}\right)} - \frac{2\pi}{\overline{n_D}\left(\overline{i}_0^{(\nu)}\right)} = 0 \\ \text{resp.}\quad & fct\left(\overline{i}_0^{(\nu)}\right) \equiv P_D\left(\overline{i}_0^{(\nu)}\right) - P_A\left(\overline{i}_0^{(\nu)}\right) = 0 \qquad \langle \nu = 1,2,3,\cdots . \end{aligned} \tag{23}$$

If for a given accuracy limit $\Delta\overline{P}$ resp. ΔP the equivalence condition

$$\left|\overline{P_A}\left(\overline{i}_0^{(\nu)}\right) - \overline{P_D}\left(\overline{i}_0^{(\nu)}\right)\right| \le \Delta\overline{P} \quad \text{resp.} \quad \left|P_A\left(\overline{i}_0^{(\nu)}\right) - P_D\left(\overline{i}_0^{(\nu)}\right)\right| \le \Delta P \tag{24}$$

is satisfied, the last inclination of the iteration process is the sought inclination $\overline{i_{QAD}} := \overline{i}_0^{(\nu)}$.

Note: An analogous procedure as in expressions (23)-(24) can be performed to compute the eccentricity $\overline{e_{QAD}}$ of an exact $\left(\overline{P_A} \triangleq \overline{P_D}\right)-$equivalence orbit while given the mean semimajor axis $\overline{a}_0$ and the mean inclination $\overline{i}_0$.

EXAMPLE 1: For a circular satellite orbit, calculate the inclination of an exact $\left(\overline{P_A} \triangleq \overline{P_D}\right)-$equivalence orbit with the semimajor axis $\overline{a}_0$ = 48000 km. Let the accuracy limits be $\Delta\overline{P} = 1.0\times10^{-10}$ sec, $\Delta\left(\overline{i}_0\right) = 1°.0\times10^{-10}$. The search step of the inclination is Δi = 0°.01, the semimajor axis Δa = 1 km. From Figure 10 the initial inclination $\overline{i}_0^{(0)}$=63°.43 is chosen.

The iteration process with the first of the condition equations (23) yields

$$\overline{i_{QAD}} = 63°.434419.$$

The corresponding mean orbital periods

$$\overline{P_A} = 104658.6978301628260 \text{ sec}, \quad \overline{P_D} = 104658.6978301628114 \text{ sec}$$

result in a posteriori accuracy $\left|\overline{P_A} - \overline{P_D}\right| = 0.1455191522837\times10^{-10}$ sec. The associated drift of the argument of the perigee is $\dot{\omega}_s$ =0.46605996438895025$\times10^{-20}$ rad/s. ◄

EXAMPLE 2: *Molniya* orbits are defined in principle by a vanishing secular drift $\dot{\omega}_s = 0.0/\sec$ of the argument of the perigee. Therefore, they can be considered as examples of $\left(\overline{P_A} \triangleq \overline{P_D}\right)-$equivalence orbits. The orbital period is usually supposed to be half a sidereal day $\overline{P_A} = \overline{P_D}$ =43082.0494520 sec and the nodal displacement per orbit should be $\overline{\Delta\lambda_\Omega}$ =-180° per mean draconitic period $\overline{P_D}$. In practice, the inclination of *Molniya* orbits is in the neighborhood of the characteristic inclination $i_{char\,1}$ =63°.434948823 in the framework of the complete *Brouwer* orbit model.

Let the semimajor axis $\bar{a}_0$ =26554.2276 km and the eccentricity $\bar{e}_0$ =0.7222 be preset. According to Figure 10 the initial value $\bar{i}_0^{(0)}$ =63°.43 can be selected for the calculation of a near-parallel $\left(\overline{P_A} \triangleq \overline{P_D}\right)-$equivalence orbit similar to a *Molniya* orbit.

$\left(\overline{P_A} \triangleq \overline{P_D}\right)$	
$\bar{a}_0$ = 26554.2276 km, $\bar{e}_0$ =0.7222, $\overline{i_{QAD}}$ =63°.423474, $\bar{\Omega}_0 = \overline{M}_{00}$ =0°, $\bar{\omega}_0$ =270°,	
$\overline{P_K}$ = 43063.714790 sec	t_0 : 2019-08-19/12:00:0.0
$\overline{P_H}$ =43069.678035 sec	P_H =43066.543233 sec
$\overline{P_A}$ = 43066.151271 sec	P_A = 43066.157842 sec
$\overline{P_D}$ = 43066.151271 sec	P_D = 43066.156528 sec
$\overline{P_T}$ = 43074.034994 sec	P_T = 43066.539103 sec
$\overline{P_R}$ = 86132.055427 sec	P_R = 86132.055427 sec
$\overline{P_S}$ = 43132.909820 sec	P_S =43069.247711 sec
$\overline{P_L}$ = 43874.623537 sec	P_L =43098.871584 sec
H_P =998.627827 km	H_A =39353.554173 km
$\overline{\Delta\lambda_P} = \dot{\lambda}_P \overline{P_A} = -179°.999484$	$\overline{\Delta\lambda_\Omega} = \dot{\lambda}_{\Omega s} \overline{P_D} = -179°.999484$
$\Delta\lambda_P = \dot{\lambda}_P P_A = -179°.999511$	$\Delta\lambda_\Omega = \dot{\lambda}_{\Omega s} P_D = -179°.999506$
$\dot{\omega}_s$ =-0. 67759598476532309×10^{-19} rad/sec	

Table 3-4: Orbital characteristics of the mean anomalistic with the mean draconitic exact equivalence orbit in the case of a Molnija-type orbit. Required accuracy $|\Delta\overline{P}| \le 10^{-10}$ sec, Δ(i)= 10^{-10} deg. Step size Δi=0°.0001. Achieved accuracy: $\left|\overline{P_A} - \overline{P_D}\right|$ =0.145519152×10^{-10} sec. Complete orbit model according to *Brouwer*. Fundamental parameters: $R_E = 6378.1366$ km, $\mu_♁ = 398600.4418$ km^3/s^2, $\dot{\Theta}$=0.72921158573340×10^{-4} / s , $J_2 = 0.001082625379977$

With the function accuracy $\Delta\overline{P} \leq 10^{-10}$ sec, the accuracy for the inclination $\Delta(i) \leq 10^{-10}$ deg and the step size Δi=0°.0001, the inclination $\overline{i_{QAD}}$ =63°.423474128 is obtained as solution of the equivalence condition (24).

The other orbital parameters are summarized in Table 3-4. The third feature of the $\left(\overline{P_A} \triangleq \overline{P_D}\right)-$equivalence orbits $\left(\overline{\Delta\lambda_P} \approx \overline{\Delta\lambda_\Omega}\right)$ is the reason why the apogee of a *Molniya* orbit (or a *Molniya* similar orbit) moves along a fixed parallel of latitude for long periods of time, analogous to the perigee. With the data chosen here, the perigee as well as the ascending node shift by about 0°.76 in two years. (Similar statements can be derived for *Tundra* orbits with one sidereal day as orbital period.). ◄

4 Near-parallel anomalistic with draconitic Equivalence Orbits

4.1 How to construct a near-parallel $\left(\overline{P_A} \triangleq \overline{P_D}\right)-$equivalence orbit

Condition (5) is an essential condition for the existence of $\left(\overline{P_A} \triangleq \overline{P_D}\right)-$equivalence orbits: A corollary is that the inclination of such an orbit must be close to the characteristic inclination $i_{char\,1}$ (or $i_{char\,2}$ resp.).

As a task, for instance, the semimajor axis $\overline{a_{QAD}}$ of a $\left(\overline{P_A} \triangleq \overline{P_D}\right)-$equivalence orbit with a given eccentricity $\overline{e}_0$ and inclination $\overline{i}_0$ should be calculated with respect to a preselected orbit model. The functional equation (6) is used for this purpose. A constructive method is to start with a suitable small first order approximation $\overline{a}_0^{(0)}$. This is then increased by a given step size Δa: $\overline{a}_0^{(\nu+1)} = \overline{a}_0^{(\nu)} + \Delta a$. At each new step, the orbital periods $\overline{P_A}, \overline{P_D}$ are calculated and compared. If the difference of the orbital periods $\left|\overline{P_A} - \overline{P_D}\right|$ depending on the respective semimajor axis $\overline{a}_0^{(\nu)}$ as independent parameter, possibly refined with the accuracy Δ(a) of the semimajor axis, falls below a specified limit value $\Delta\overline{P}$

$$\left|\overline{P_A}\left(\overline{a}_0^{(\nu)}, \overline{e}_0, \overline{i}_0\right) - \overline{P_D}\left(\overline{a}_0^{(\nu)}, \overline{e}_0, \overline{i}_0\right)\right| < \Delta\overline{P} \quad \langle \nu = 0,1,2,3,\cdots, \tag{25}$$

the last obtained value $\overline{a}_0^{(\nu)} =: \overline{a_{QAD}}$ can be regarded as the semimajor axis of a $\left(\overline{P_A} \triangleq \overline{P_D}\right)-$equivalence orbit. This value is therefore essentially a function of the step size Δa, the specified function accuracy $\Delta\overline{P}$, the specified accuracy of the semimajor axis Δ(a) and the permitted orbit model.

How can it be proved that a $\left(\overline{P_A} \triangleq \overline{P_D}\right)-$equivalence orbit is a near-parallel $\left(\overline{P_A} \triangleq \overline{P_D}\right)-$equivalence orbit?

If it is not known from other considerations that an orbit with a given orbit model is a near-parallel $\left(\overline{P_A} \triangleq \overline{P_D}\right)$ – orbit, one can approach such an orbit step by step. Given are the mean eccentricity $\overline{e}_0$ and the mean inclination $\overline{i}_0$ of the searched orbit, whose semimajor axis $\overline{a_{QAD}}$ is to be determined as that of a $\left(\overline{P_A} \triangleq \overline{P_D}\right)$ – equivalence orbit.

$\Delta\overline{P}$ [sec]	J_2, J_4	$\overline{a}_0$ [km]	H_P [km]	$\left(\overline{P_a} - \overline{P_d}\right)$ [sec]	$\dot{\omega}_s$ [rad/sec]	Q
10^{-2}	J_2, J_4	10120.210154	200.000	0.1256×10^{-3}	$-0.7682459 \times 10^{-11}$	N*
10^{-2}	J_2	10120.210154	200.000	0.5011×10^{-2}	0.306629×10^{-9}	N*
10^{-3}	J_2, J_4	10120.210154	200.000	0.1256×10^{-3}	$-0.7682460 \times 10^{-11}$	N*
10^{-3}	J_2	255289.210154	200.000	0.9999×10^{-3}	$0.3812937 \times 10^{-14}$	N*
10^{-4}	J_2, J_4	10146.210769	216.900	0.9907×10^{-4}	$-0.601542 \times 10^{-11}$	N
10^{-4}	J_2	No convergence				
10^{-8}	J_2, J_4	10245.888986	281.691	$<10^{-8}$	$-0.9485177 \times 10^{-21}$	E
10^{-8}	J_2	No convergence				

Table 4-1: Selection of the semimajor axis $\overline{a_{QAD}}$ of $\left(\overline{P_A} \triangleq \overline{P_D}\right)$ – equivalence orbits with epoch elements $\overline{e}_0$ =0.35 and $\overline{i}_0$ =63°.418. $\left|\overline{P_A} - \overline{P_D}\right| = \Delta\overline{P}$ is the required accuracy. For the search of the corresponding semimajor axes the step size Δa = 1 km with the accuracy limit Δ(a) $\leq 10^{-7}$ km was chosen. <N*> denotes an orbit with perigee height H_P = 200 km (initial value of the search process), <N> orbit with perigee height of H_P > 200 km, <E> exact equivalence orbit with perigee greater than 200 km.

One starts with the assumption of a $\left(\overline{P_A} \triangleq \overline{P_D}\right)$ – exact equivalence orbit with the accuracy limit $\Delta\overline{P} = 10^{-8}$sec (or even finer). If the orbit is not an exact $\left(\overline{P_A} \triangleq \overline{P_D}\right)$ – equivalence orbit, the iteration to calculate the semimajor axis will not converge. In the next step, with reduced accuracy limit $\Delta\overline{P}$ sec, the iteration process is repeated. This process is repeated until the computational process converges and a semimajor axis is obtained. According to experience, a useful satellite orbit in the case of an orbit model, which only includes the orbit influences by the J_2-harmonic, can be obtained only from the accuracy limit $\Delta\overline{P} = 10^{-3}$sec and coarser.

Table 4-1 shows a numerical example with parameters $\bar{e}_0$=0.35, and inclination $\bar{i}_0$=63°.418, i.e. below the characteristic inclination $i_{char\,1}$. If the orbit model with the J_2-harmonic alone is used, the semimajor axis $\bar{a}_0$=255289.210154 km results in the case $\Delta\bar{P}=10^{-3}$sec. This is in the application case of Earth satellites without interest.

If, on the other hand, the whole *Brouwer* orbital model with J_2 and J_4 is admitted, an orbit with the semimajor axis $\bar{a}_0$=10120.210154 km results with the accuracy $\Delta\bar{P}=10^{-3}$sec. This amount is also obtained if only the accuracy $\Delta\bar{P}=10^{-2}$sec is admitted. The reason is that this quantity is the first approximate quantity for the iteration process, which is obtained with the given eccentricity with respect to the minimum perigee height H_P=200 km: $\bar{a}_0^{(0)}=\left(R_E+H_P\right)/\left(1.0-\bar{e}_0\right)$. It is remarkable that in the case $\Delta\bar{P}=10^{-2}$sec there is no difference between the orbit models with and without J_4 in the result. In both cases the required accuracy is already fulfilled with the initial approximation.

These considerations are the basis for the empirical value that near-parallel $\left(\overline{P_A}\triangleq\overline{P_D}\right)-$equivalence orbits can typically be considered with the accuracy limit $\Delta\bar{P}=10^{-2}$sec.

In Table 4-1 it is also noticeable that the numerical value for the secular drift $\dot{\omega}_{Gs}$ of the argument of the perigee is always positive in the case of the orbit model with J_2 alone, and always negative in the case of the orbit model inclusive J_2 and J_4. Here, the sign of the J_4-component $\dot{\omega}_{Gs/4}$ from formula (21) is of influence.

Altogether, the following conclusion is obvious: also, a simple orbit model (in the current case with J_2 alone) can lay out a useful orbit. A more refined orbit model (in the current case with J_2 and J_4) can under certain circumstances (e.g. other certain orbit parameters, such as inclination) provide other fundamental statements. Therefore, it remains an open question whether even more sophisticated orbital models (in the current case those that go beyond *Brouwer*'s orbital model) must be expected to yield new statements that are not foreseeable at first. These statements only concern problems of orbit design.

However, the problem of an orbit model for use in an ephemeris is of no interest in the existing task area and is therefore not considered in the present study.

4.2 Illustration of near-parallel $\left(\overline{P_A}\triangleq\overline{P_D}\right)-$equivalence orbits

Figure 11 illustrates some examples of the variety of near-parallel $\left(\overline{P_A}\triangleq\overline{P_D}\right)-$equivalence orbits. Starting from given inclinations (with one exception only inclinations larger than the characteristic inclination $i_{char\,1}$), the course of the semimajor axis is plotted versus the eccentricity in the interval $e\in\left[0.00,0.96\right]$ with a step size of Δe=0.001. To satisfy the boundary conditions necessary to obtain the corresponding orbital periods, the semimajor axis is calculated with the step size Δa=1 km. The curves are calculated with the whole *Brouwer* model J_2, J_3, J_4 (i.e. inclusive all periodic perturbations).

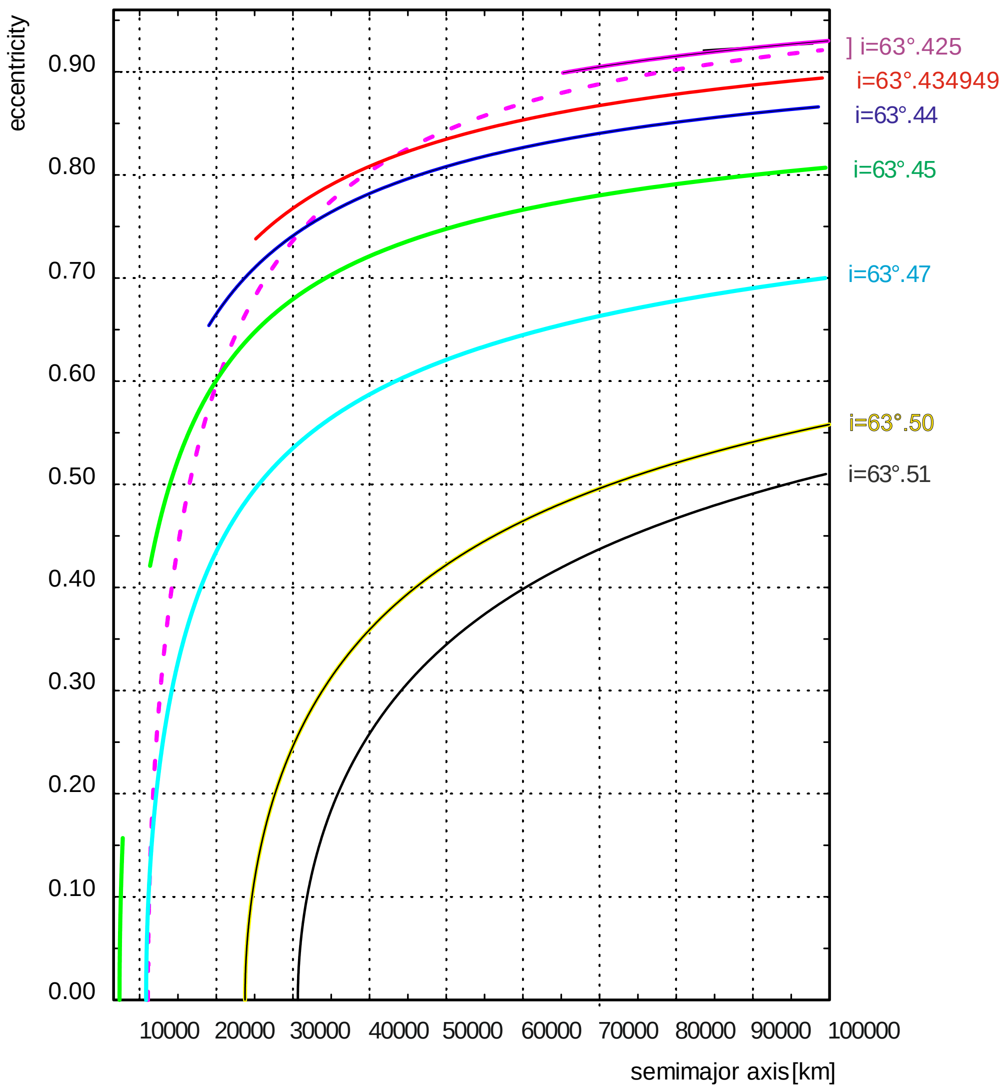

Figure 11: The relation between eccentricity and semimajor axis of near-parallel $\left(\overline{P_A} \triangleq \overline{P_D}\right)$ – equivalence orbits for different orbital inclinations, calculated the full *Brouwer* orbital model. Step sizes Δa = 1 km, Δe = 0.001, minimum orbital altitude H_P = 200 km, accuracies $\Delta(a)\times 10^{-8}$ km and $\left|\Delta\overline{P}\right|$ <0.01 sec, $\Delta(a)<10^{-6}$ km, $\Delta(e)<10^{-6}$. The green curve for i=63°.45 is interrupted between the (a, e)-points (7804,0.157) - (11366,0.421) because the minimum orbital altitude reached there is below the allowed H_P =200 km. Note that for $\overline{i_0}$ = 63°.425 a short curve for a near-parallel $\left(\overline{P_a} \triangleq \overline{P_d}\right)$ – equivalence orbit is obtained with accuracy 0.01 sec. For a comparison, the long dotted $\overline{i_0}$ = 63°.425 curve shows an exact $\left(\overline{P_a} \triangleq \overline{P_d}\right)$ – equivalence orbit with accuracy 10^{-9} sec. [A similar plot was firstly published in (Jochim 2020) Figure 8]

An exception is the examination for the inclination $\overline{i_0}$ =63°.425. According to Figure 10 it can be seen (by extrapolation to $\overline{e}_0$=0.95) that it is an exact $\left(\overline{P_A} \triangleq \overline{P_D}\right)$ – equivalence orbit. It is calculated with the accuracy $\Delta\overline{P} < 10^{-9}$ sec. The corresponding curve is drawn dotted in Figure 11. In this case, the equivalence orbit has the semimajor axis $\overline{a_{QAD}}$ =97787.158916 km for the eccentricity $\overline{e}_0$ =0.92.

However, if a near-parallel equivalence orbit is desired for inclination $\bar{i}_0$ =63°.425 and eccentricity $\bar{e}_0$ =0.92 with accuracy $\Delta\bar{P} < 10^{-2}$ sec, the corresponding semimajor axis is $\overline{a_{QAD}}$ =85685.707500 km. The difference between the two orbits with the same inclination can be clearly seen in Figure 11.

EXAMPLE: The semimajor axis of a retrograde $\left(\overline{P_A} \triangleq \overline{P_D}\right)-$equivalence orbit with the inclination =116°.6, thus in the environment of the second characteristic inclination $i_{char\ 2}$, is to be constructed. The inclination is thus in a range, in this case below $i_{char\ 2}$, in which according to the previous considerations only a near-parallel $\left(\overline{P_A} \triangleq \overline{P_D}\right)-$equivalence orbit can exist. Therefore, the accuracy limit $\Delta\bar{P} = \left|\overline{P_A} - \overline{P_D}\right| < 10^{-2}$ sec is required. The eccentricity should be $\bar{e}_0 = 0.35$.

$\left(\overline{P_A} \triangleq \overline{P_D}\right)$	
$\overline{a_{QAD}} = 10120.210154$ km, $\bar{e}_0 = 0.35$, $\bar{i}_0 = 116°.6$, $\bar{\Omega}_0 = 0°$, $\bar{\omega}_0 = 0°$, $\overline{M_{00}} = 0°$	
$\overline{P_K} = 10132.002239$ sec	t_0 : 2021-02-10/12:00:0.0
$\overline{P_A} = 10133.586758$ sec	$P_A = 10133.586758$ sec
$\overline{P_D} = 10133.581553$ sec	$P_D = 10133.581553$ sec
$\overline{P_R} = 9070.247932$ sec	$P_R = 9281.450392$ sec
$H_P = 200.0$ km	$H_A = 7284.147108$ km
$\overline{\Delta\lambda_P} = \dot{\lambda}_P \overline{P_A}$ = -42°.204034	$\overline{\Delta\lambda_\Omega} = \dot{\lambda}_{\Omega s} \overline{P_D}$ = -42°.203929
$\Delta\lambda_{Ps} = \dot{\lambda}_P P_A$ = -42°.204034	$\Delta\lambda_{\Omega s} = \dot{\lambda}_{\Omega s} P_D$ = -42°.203929
$\dot{\Omega}_s = 0.23239382460156005 \times 10^{-6}$ rad/s	
$\dot{\omega}_s = 0.31849305643123630 \times 10^{-9}$ rad/sec	
$(M_0)^{\bullet}_s = -0.96965887079983346 0\times 10^{-7}$ rad/s	

Table 4-2: Orbital properties of a near-parallel retrograde $\left(\overline{P_A} \triangleq \overline{P_D}\right)-$ equivalence orbit with inclination $\bar{i}_0$ = 116°.6 and eccentricity $\bar{e}_0$ = 0.35. The calculation of the orbit uses the whole *Brouwer* orbit model. Step size Δa= 1km, preset limit accuracies $\Delta\bar{P} = \left|\overline{P_A} - \overline{P_D}\right| \le 10^{-2}$ sec, $\Delta(a) \le 10^{-7}$ km. Fundamental parameters: $R_E = 6378.1366$ km, $\mu_♁ = 398600.4418$ km^3/s^2, $\dot{\Theta}$=0.72921158573340$\times 10^{-4}$ /s, J_2 = 0.001082625379977. The numbers highlighted in green indicate the near-parallel equivalence.

The result of the search process is a near-parallel $\left(\overline{P_A} \triangleq \overline{P_D}\right)-$equivalence orbit with the achieved accuracy $\left|\overline{P_A} - \overline{P_D}\right| = 0.5205306855714 \times 10^{-2}$ sec. The calculated orbit parameters are summarized in Table 4-2. This orbit also satisfies (with limited but tolerable accuracy over long periods of time) the second condition (17): Both perigee and apogee move along a fixed parallel of latitude over long time intervals.

Note the relatively small value for the meridional periods $\overline{P_R}$, P_R on the retrograde orbit. After a meridional orbit $\overline{P_R}$, the satellite passes over the same reference meridian before it can coincide with the other reference orbital points such as perigee, nodal points, etc... The true orbital periods P_A, P_D, except for the true meridional period P_R, are identical to the corresponding mean orbital periods $\overline{P_A}, \overline{P_D}$. This is a consequence of the low accuracy 10^{-2} sec required. The search process for the true near-parallel $\left(\overline{P_A} \triangleq \overline{P_D}\right)-$equivalence orbit ends at the first approximate solution below the required minimum accuracy. It also shows the minimum altitude 200 km.

4.3 On the smooth transition from exact to near-parallel $\left(\overline{P_A} \triangleq \overline{P_D}\right)-$equivalence orbits

The transition in the current case of a hybrid-$\left(\overline{P_A} \triangleq \overline{P_D}\right)-$equivalence orbit between the possible range of the exact $\left(\overline{P_A} \triangleq \overline{P_D}\right)-$equivalence orbit and the possible range of the near-parallel $\left(\overline{P_A} \triangleq \overline{P_D}\right)-$equivalence orbit is not abrupt but gradual, depending on the increasing tolerance threshold $\Delta\overline{P}$. This is shown in the sequence of Figure 12 - Figure 15, where always the full *Brouwer*'s orbit model is applied. Starting from the overview of possible exact equivalence orbits in Figure 10, the tolerance threshold $\Delta\overline{P}$ for generating the area of possible near-parallel $\left(\overline{P_A} \triangleq \overline{P_D}\right)-$equivalence orbits is increased from image to image. This systematically causes a shift of the area of possible equivalence orbits in the direction of ascending inclinations beyond the characteristic inclination $i_{char\,1}$.

In the $\Delta\overline{P} \le 10^{-2}$sec case, i.e., the typical case of near-parallel $\left(\overline{P_A} \triangleq \overline{P_D}\right)-$equivalence orbits, the region of possible equivalence orbits has almost completely moved beyond the characteristic inclination $i_{char\,1}$. If the tolerance is further increased, the region of possible $\left(\overline{P_A} \triangleq \overline{P_D}\right)-$equivalence orbits gradually becomes diffuse and there are then also additional possible near-parallel $\left(\overline{P_A} \triangleq \overline{P_D}\right)-$equivalence orbits below $i_{char\,1}$. The larger the tolerance threshold, the less pronounced is the boundary curve with the limit value e_B of eccentricity when the orbits are referenced to the minimum perigee height H_P =200 km.

In all Figures 12-16, the step sizes $\Delta a = 1\text{km}$, $\Delta i = 0°.0001$, $\Delta e = 0.01$, were used for the calculations performed with the full *Brouwer* orbital model (Only Figure 16 uses secular perturbations only).

The curve e_B shows the possible limit of eccentricity with respect to the minimum perigee height $H_{P,\min}$ =200 km. The color coding of the individual curves matches in all images.

Finally, in the case of the tolerance threshold $\Delta\overline{P} \le 1\sec$, the boundary curve is no longer discernible, the region of possible near-parallel $\left(\overline{P_A} \triangleq \overline{P_D}\right)-$equivalence orbits extending on both sides of the characteristic inclinations. In Figure 16 the vicinity of the second characteristic inclination $i_{char\,2}$ is additionally shown as well.

Figure 10 confirms the statement: $\left(\overline{P_A} \triangleq \overline{P_D}\right)-$exact equivalence orbits are restricted to inclinations smaller than the characteristic inclination $i_{char\,1}$. (Mirror image statement for inclinations larger than the characteristic inclination $i_{char\,2}$). Figure 14 shows the range of possible near-parallel $\left(\overline{P_A} \triangleq \overline{P_D}\right)-$equivalence orbits for the accuracy limit $\Delta\overline{P} = \left|\overline{P_a} - \overline{P_d}\right| \le 10^{-2}\sec$, which is typical for near-Earth near-parallel-$\left(\overline{P_A} \triangleq \overline{P_D}\right)-$equivalence orbits as derived in the previous considerations. Nearly all orbits in this region have inclinations above the characteristic inclination $i_{char\,1}$. Exceptions exist only for some highly eccentric orbits, as exemplified by the orbit with inclination $\bar{i}_0$ =63°.425 in Figure 11. Figure 2 shows furthermore: If a reduced orbit model is used, which allows only impacts by the harmonic J_2, no exact $\left(\overline{P_A} \triangleq \overline{P_D}\right)-$equivalence orbits can be found at all.

- *Typicall for hybrid equivalence orbits is the smooth transition from exact to near-parallel equivalence orbits.*

So far, no other equivalence orbit has been found for which such fundamentally different behavior can be demonstrated for different orbit models and different parameter ranges. (Up to now, 42 different kinds of equivalence orbits have been investigated in detail outside the present study.)

Summarizing the last considerations, we obtain, using *Brouwer*'s orbit model,

- *the **fourth property of** $\left(\overline{P_A} \triangleq \overline{P_D}\right)-$**equivalence orbits**: Orbits calculated with the full Brouwer orbit model are exact $\left(\overline{P_A} \triangleq \overline{P_D}\right)-$equivalence orbits if their inclination is below the characteristic inclination $i_{char\,1}$. Nearly all near-parallel $\left(\overline{P_A} \triangleq \overline{P_D}\right)-$equivalence orbits with the accuracy limit $\Delta\overline{P} = \left|\overline{P_a} - \overline{P_d}\right| \le 10^{-2}\sec$ have inclinations above the characteristic inclination $i_{char\,1}$. With a reduced orbit model taking into account the orbit influences by the harmonic J_2 alone, no exact $\left(\overline{P_A} \triangleq \overline{P_D}\right)-$equivalence orbits can be found. These statements can be applied in a mirror-image way also for the second characteristic inclination $i_{char\,2}$.*

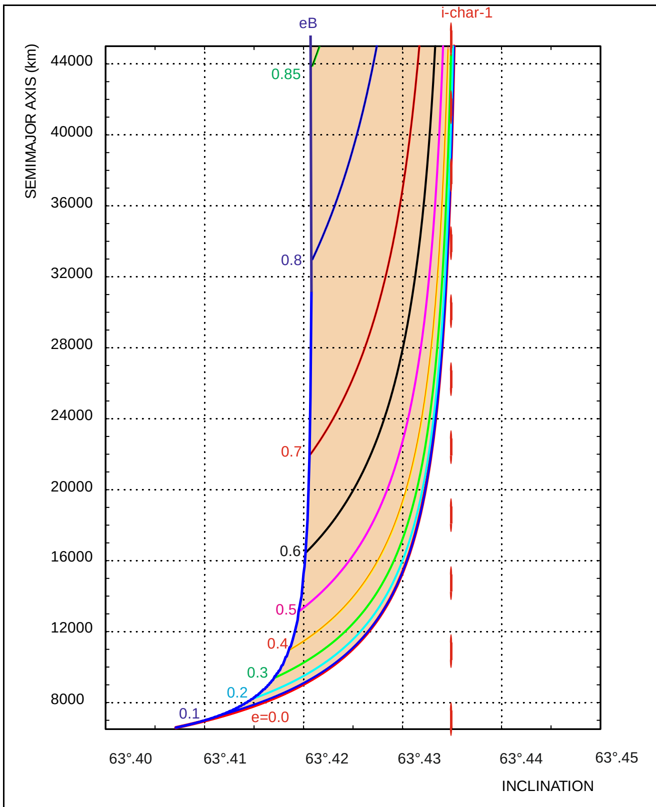

Figure 12 : threshold $\Delta\overline{P} = \left|\overline{P_A} - \overline{P_D}\right| \leq 10^{-4}$ sec

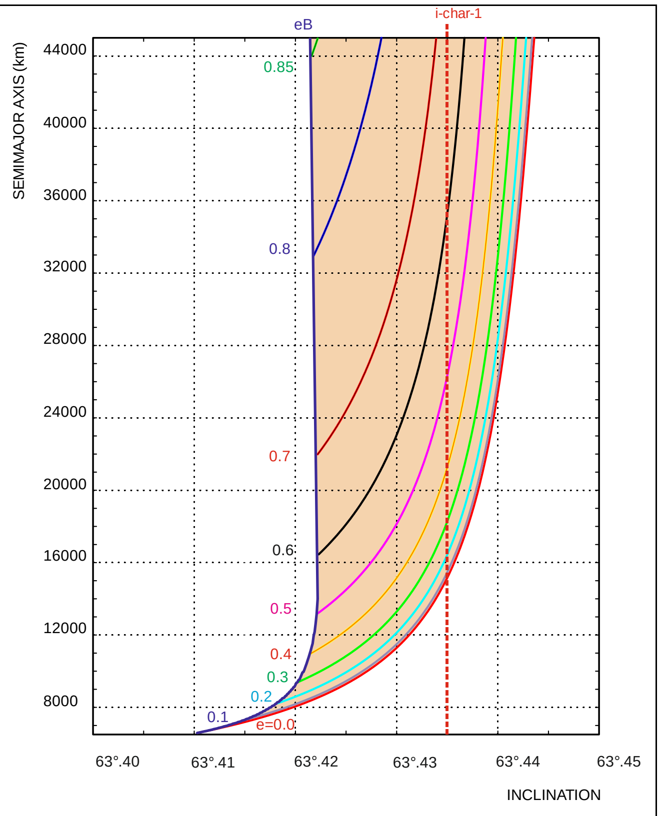

Figure 13 : threshold $\Delta\overline{P} = \left|\overline{P_A} - \overline{P_D}\right| \leq 10^{-3}$ sec

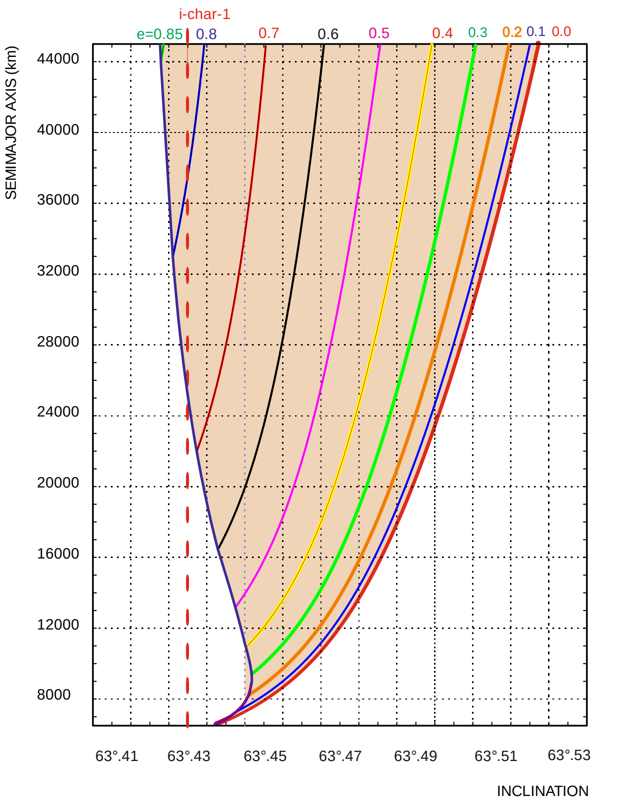

Figure 14 : threshold $\Delta\overline{P} = \left|\overline{P_A} - \overline{P_D}\right| \leq 0.01$sec

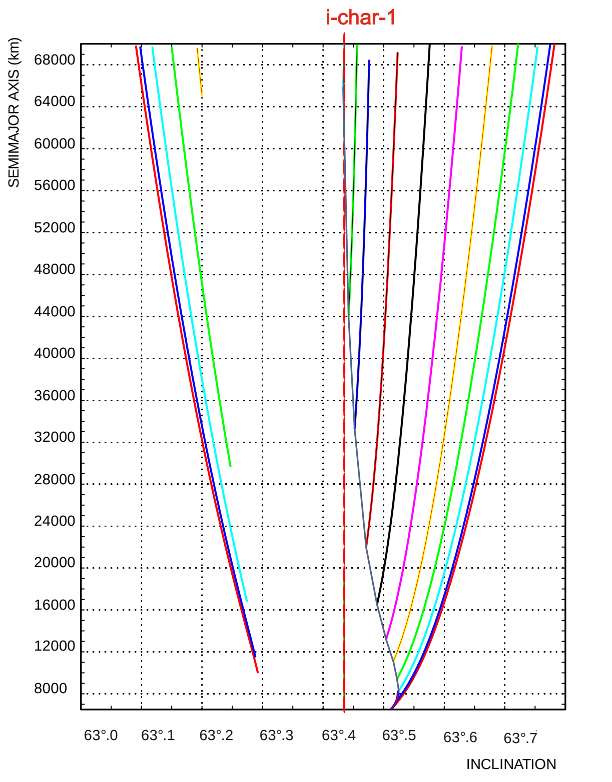

Figure 15: threshold $\Delta\overline{P} = \left|\overline{P_a} - \overline{P_d}\right| \leq 0.03$sec ,

Figure 16 : Overview of possible near-parallel $\left(\overline{P}_a \triangleq \overline{P}_d\right)$ – equivalence orbits semimajor axis versus the inclination for some eccentricities $e \in \left[0.0 - 0.85\right)$. Tolerance $\Delta\overline{P} = \left|\overline{P}_a - \overline{P}_d\right| \leq 1\,\text{sec}$ is allowed as accuracy. The orbit model includes only secular perturbations due to J_2, J_4. The calculation is performed with the step sizes $\Delta a = 10\,\text{km}$, $\Delta i = 0^{\circ}.1$, $\Delta e = 0.01$. The color coding of the curves of possible equivalence orbits corresponds in all cases to the indicated above the left image area.

5 Summary and Implications

The research presented in this paper can be summarized in the following conclusions:

1. The coupling of two or more satellite motions can lead to orbits with very special properties. These orbits are called equivalence orbits. They are sometimes extremely stabilized orbits. Therefore, many of these orbits are of special interest for practical applications.
2. In the present study, equivalence orbits are derived exclusively with the *Brouwer*'s analytical orbit model (Brouwer, 1959). This allows general statements to be obtained. These can then be refined and updated in a special application case with an extended orbit model, in particular by comprehensive numerical integration. A classification by altitude range (e.g. LEO, MEO, GEO, HEO etc.) is not useful in this context, because highly eccentric orbits penetrate all these altitude ranges and thus different orbital influences.
3. Exact equivalence orbits require the use of a complete orbit model of second or higher order.
4. Using the analytical *Brouwer* orbit model, the condition equations of the $\left(\overline{P_A} \triangleq \overline{P_D}\right)-$equivalence orbits necessarily lead to first order characteristic inclinations $i_{char\,1}$ and $i_{char\,2}$. In the present context of $\left(\overline{P_A} \triangleq \overline{P_D}\right)-$equivalence orbits, these characteristic inclinations are identical with the critical inclinations.
5. $\left(\overline{P_A} \triangleq \overline{P_D}\right)-$equivalence orbits are called exact $\left(\overline{P_A} \triangleq \overline{P_D}\right)-$equivalence orbits if the difference between their orbital periods vanishes (e.g. with condition limit $0 \le \left|\overline{P_A} - \overline{P_D}\right| < 10^{-9}\,\text{sec}$). If the difference never vanishes but can fall below a small accuracy limit (e.g. with condition limit $0 \le \left|\overline{P_A} - \overline{P_D}\right| < 10^{-2}\,\text{sec}$), these equivalence orbits are called near-parallel $\left(\overline{P_A} \triangleq \overline{P_D}\right)-$equivalence orbits. Surprisingly, $\left(\overline{P_A} \triangleq \overline{P_D}\right)-$equivalence orbits are not only exact $\left(\overline{P_A} \triangleq \overline{P_D}\right)-$equivalence orbits for inclinations smaller than the characteristic inclination $i_{char\,1}$ depending on the orbital model used, but also near-parallel $\left(\overline{P_A} \triangleq \overline{P_D}\right)-$equivalence orbits for inclinations mostly larger than the characteristic inclination $i_{char\,1}$. For this reason, $\left(\overline{P_A} \triangleq \overline{P_D}\right)-$equivalence orbits are also called hybrid-$\left(\overline{P_A} \triangleq \overline{P_D}\right)-$equivalence orbits.
6. The required accuracy limit $0 \le \left|\overline{P_A} - \overline{P_D}\right| < 10^{-9}\,\text{sec}$ in the case of exact $\left(\overline{P_A} \triangleq \overline{P_D}\right)-$equivalence orbits is a general empirical value obtained from numerous calculations. It can be substantially exceeded in the case of mean equivalence orbits.

7. In the case of true $\left(P_A \triangleq P_D\right)$ – equivalence orbits this bound can often be reached only with difficulty. Reasons can be the lengthy iterations, step sizes Δa, Δe, Δi too small, numerical restrictions, programming inaccuracies, computer limitations.

   For near-parallel $\left(\overline{P_A} \triangleq \overline{P_D}\right)$ – equivalence orbits the reasonable accuracy limit 10^{-2} results from the observation that the curves of the orbital periods versus the semimajor axis of the two considered types of motion never overlap, but approach each other more and more with increasing semimajor axis. In the near-Earth range, approximately up to geosynchronous orbits, the size 10^{-2} sec can be regarded as typical according to experience. Smaller limits are reached only for such high orbits, e.g. 70000 km and higher, as they do not seem reasonable for the usual ranges of a satellite orbit analysis.

8. $\left(\overline{P_A} \triangleq \overline{P_D}\right)$ – equivalence orbits are of great practical interest. The reason for this is the linkage of the shift of the geographic longitude of the ascending node with the shift of the geographic longitude of the perigee. This effect stabilizes the orbit with respect to the Earth's surface. For long time intervals, in the range of many years, the perigee (analogously the apogee) of the satellite orbit moves along a fixed parallel of latitude.

9. The selection of a $\left(\overline{P_A} \triangleq \overline{P_D}\right)$ – as well as a $\left(P_A \triangleq P_D\right)$ – equivalence orbits is characterized by the orbit model used, the specification of the step sizes $\Delta a, \Delta i, \Delta e$, the required accuracy Δ(a), Δ(e), Δ(i) of the orbit elements and the condition function $\Delta fct \equiv \left|\overline{P_A} - \overline{P_D}\right| \le \Delta\overline{P}$. $\Delta\overline{P}$ is a certain fixed value for the required accuracy.

10. An equivalence orbit enforces the motion of a satellite on an orbit that identically satisfies the behavior of two relative motions. In this sense, a surprising property can be observed when one of the motions considered is the *Kepler*ian motion. *Kepler*ian motion is normally considered to be "unperturbed" motion and is therefore of theoretical interest only. However, if it were possible to balance the *Kepler*ian motion with another relative motion, this second motion would force the satellite into a *Kepler*ian orbit. In this case, the unavoidable orbital influences ("perturbations") would cause the satellite to move on an apparently "undisturbed" orbit. This is the case at least for mean satellite motions. (Examples of this are examined outside of this study).

11. Combining different satellite motions into equivalence orbits can in many cases result in extremely long-term orbit stability (in the range of many years). Examples are presented in an earlier paper (Jochim 2020).

12. In general, astrodynamic investigations should be checked whether different orbital models, different numerical calculation methods and different physical orbital disturbances ("orbital perturbations") can lead to different results in principle.

6 References

BREAKWELL, J. V. (1959) 'On the Anomalies in the Movement of the Perigee due to Oblateness and Air Drag for Critical Values of the Inclination', *Proceedings of the NASA Conference on Orbit and Space Trajectory Determination*

BROUWER, D. (1959) 'Solution of the Problem of Artificial Satellite Theory without Drag', *Astronomical Journal* **64**, 378–397

Jochim, E. F. M. (2012) 'The Significance of the Hansen Ideal Space Frame', *Astron. Nachr*. / AN **333**, No. 8, 774-783 (2012) / **DOI** 10.1002/asna.202222711

JOCHIM, E. F.M (2018): *Satellitenbewegung, Band IV, Bewegungsanalyse* (Satellite Motion, Vol. IV.: Satellite Orbit Analysis), ISRN DLR FB 2018-31, ISSN 1434-8454

JOCHIM, E. F. M. (2020) 'Satellite Equivalence Orbits', *Acta Astronautica* 179 (2021), 213-227 (https://doi.org/10.1016/j.actaastro,2020.10.045, Available online 1 November 2020, 0094-5765/© 2020 Published by Elsevier Ltd on behalf of IAA)

KAULA, W. M. (1966): *Theory of Satellite Geodesy, Applications of Satellites to Geodesy*, Blaisdell Publishing Company, Waltham, Mass. – Toronto – London

KLINKRAD, H. (1985) 'Orbit Design of the First ESA Remote Sensing Satellite ERS-1', IAF-85-254

URBAN, SEAN E. and P. KENNETH SEIDELMANN, (eds.) (2013) *Explanatory Supplement to The Astronomical Almanac*, 3rd ed., University Science Books, Mill Valley, CA, ISBN 978-1-891389-85-6

http://asa.usno.navy.mil/: Astronomical_Constants_2017.pdf

https://de.wikipedia.org/wiki/Molnija: *English spelling sometimes Molniya or Molnyia*.

Acknowledgments:

The paper is dedicated to *Dr. med. Gertrud Jochim* with deep gratitude for her daily support and care.

The author cordially thanks to the two unknown Celestial Mechanics referees for their competent and constructive qualification, to *Dr. Ing. Mark Lützner* for his valuable, critical and constructive support in the compilation of this paper, to *Dipl. Ing. Manfred Hager* and *Dipl. Ing. Simon Krebietke* for the difficult and expensive maintenance of the computer after implementation of the new MS system update. He is indebted to the director of the Microwave and Radar Institute of DLR, *Prof. Dr. Ing. habil Alberto Moreira*, and the department head *Dr. Ing. Thomas Neff* for their encouragement of my work as well as for the support by the use of the institute's infrastructure and computers.